Transverse impedance studies of 2D azimuthally symmetric devices of finite length

N. Biancacci,[1] A. Passarelli,[2] V. G. Vaccaro,[2] E. Métral,[1] B. Salvant,[1] M. Migliorati,[3] and L. Palumbo[3]

[1]*CERN, 1211 Geneva 23, Switzerland*
[2]*INFN Naples Unit, Via Cintia, 80126 Napoli, Italy*
[3]*Rome University "La Sapienza," Piazzale Aldo Moro 5, 00185 Roma, Italy*

(Received 22 December 2022; accepted 20 March 2023; published 13 April 2023)

The accurate calculation of the beam coupling impedance for particle accelerators is necessary to carefully assess the machine stability against impedance-driven collective effects. A first order evaluation of the beam coupling impedance is often done by means of analytical formulas and/or 2D numerical codes. The infinite length approximation is often used to simplify the calculation of the beam coupling impedance of accelerator elements. This is expected to be a reasonable assumption for devices whose length is greater than the transverse dimension but may be a less accurate approximation for segmented devices. In this work, we present the application of the mode matching method to the calculation of the transverse dipolar impedance of a cylindrical cavity loaded with a toroidal insert. By choosing different insert electromagnetic properties (permittivity, permeability, and conductivity) and dimensions, the model can represent a beam pipe, a thin insert, a lossy cavity, or a collimator for which the effect of the finite length is investigated. The method is successfully benchmarked against available analytical formulas, field-matching codes, and 3D commercial solvers. The proposed model allows for performing wide parametric scans and reaching accurate results, therefore becoming an essential tool for the impedance evaluation of accelerator devices.

DOI: 10.1103/PhysRevAccelBeams.26.042001

I. INTRODUCTION

The impedance evaluation of finite length devices, in particular simple cavities, has been mainly approached by means of the field matching technique [1–6], i.e., imposing the electric and magnetic fields continuity at the boundaries between the finite length device and the incoming and outgoing beam pipes or by means of numerical methods [7–11]. In our previous work [12], we rigorously studied the longitudinal beam coupling impedance of a cavity loaded with a generic linear, isotropic, stationary, dispersive, homogenous, toroidal material, by means of the mode matching method [13,14], which is based on the modal expansion of the cavity fields whose coefficients can be directly related to the external fields at the interfaces. The present study focuses on the evaluation of the transverse dipolar impedance, complementing the work of [12] to develop a new tool for the impedance evaluation of accelerator devices.

This paper is divided into three parts: in Sec. II, we recall the theoretical background of the mode matching method; in Sec. III, we derive the electromagnetic fields scattered in the structure; in Sec. IV, we show the applications and benchmarks for significant cases in accelerators. We compare our model with the classical thick wall formula for resistive wall impedance and with a commercial particle wakefield simulator. The impedance dependency on the device length will be also studied in order to assess the validity of the usual "infinite length" approximation and to characterize the presence of trapped modes. Since the used approach is non-ultrarelativistic, we also study the impedance behavior as a function of the relativistic particle beam velocity.

II. THEORETICAL BACKGROUND

In this section, we show the expressions of the electromagnetic field decomposition in a closed volume. The derived equations are the basis for the mode matching method.

Given a volume V, enclosed in an ideal surface $S = S_E \cup S_H$, with S_E perfect electric, and S_H perfect magnetic boundary surfaces, the scattered electromagnetic fields $\bar{E}$ and $\bar{H}$ may be decomposed by means of the Helmholtz theorem in summation of irrotational and solenoidal modes which constitute a complete set of orthonormal functions [13,14]. We can write

TABLE I. Eigenvector equations.

Eigenvector	In V	On $S = S_E \cup S_H$
$\bar{e}_n$	$\nabla \times \bar{e}_n = k_n \bar{h}_n$	$\begin{cases} \hat{n}_0 \times \bar{e}_n = 0; & \text{on } S_E \\ \hat{n}_0 \cdot \bar{e}_n = 0; & \text{on } S_H \end{cases}$
$\bar{f}_n = \nabla \Phi_n$	$\nabla^2 \Phi_n + \mu_n^2 \Phi_n = 0$	$\begin{cases} \Phi_n = 0; & \text{on } S_E \\ \partial \Phi_n / \partial n = 0; & \text{on } S_H \end{cases}$
$\bar{h}_n$	$\nabla \times \bar{h}_n = k_n \bar{e}_n$	$\begin{cases} \hat{n}_0 \cdot \bar{h}_n = 0; & \text{on } S_E \\ \hat{n}_0 \times \bar{h}_n = 0; & \text{on } S_H \end{cases}$
$\bar{g}_n = \nabla \Psi_n$	$\nabla^2 \Psi_n + \nu_n^2 \Psi_n = 0$	$\begin{cases} \partial \Psi_n / \partial n = 0; & \text{on } S_E \\ \Psi_n = 0; & \text{on } S_H \end{cases}$

$$\bar{E} = \sum_n \mathbf{V}_n \bar{e}_n + \sum_n \mathbf{F}_n \bar{f}_n, \tag{1}$$

$$\bar{H} = \sum_n \mathbf{I}_n \bar{h}_n + \sum_n \mathbf{G}_n \bar{g}_n, \tag{2}$$

where $\bar{e}_n$ and $\bar{h}_n$ are solenoidal and $\bar{f}_n$ and $\bar{g}_n$ irrotational orthonormal eigenvectors.

Table I summarizes the eigenvectors together with their corresponding differential equations and boundary conditions. In this formulation, $\hat{n}_0$ is the unit vector normal to S pointing internally to the volume, while k_n, μ_n, and ν_n represent the eigenvalues corresponding to the eigenvectors.

Since the eigenvectors are determined by the geometry of the structure under study, the problem reduces to finding the coefficients $\mathbf{V}_n$, $\mathbf{F}_n$, $\mathbf{I}_n$, and $\mathbf{G}_n$. For the reader's convenience, we report the expression of the expansion coefficients already derived in [12] with $Z_o = 1/Y_o$, the characteristic impedance and $k = \omega/c$, the propagation constant in vacuum, with $\omega = 2\pi f$, the angular frequency.

$$\mathbf{I}_n = \frac{1}{k^2 - k_n^2}\left(jkY_0 \int_{S_E} (\bar{E} \times \bar{h}_n^*) \cdot \hat{n}_0 \mathrm{d}S - k_n \int_{S_H} (\bar{e}_n^* \times \bar{H}) \cdot \hat{n}_0 \, \mathrm{d}\, S \right), \tag{3}$$

$$\mathbf{V}_n = \frac{1}{k^2 - k_n^2}\left(jkZ_o \int_{S_H} (\bar{e}_n^* \times \bar{H}) \cdot \hat{n}_0 \mathrm{d}S + k_n \int_{S_E} (\bar{E} \times \bar{h}_n^*) \cdot \hat{n}_0 \, \mathrm{d}S \right), \tag{4}$$

$$\mathbf{G}_n = j \frac{Y_0}{k} \int_{S_E} (\bar{E} \times \bar{g}_n^*) \cdot \hat{n}_0 \, \mathrm{d}S, \tag{5}$$

$$\mathbf{F}_n = -j \frac{Z_o}{k} \int_{S_E} (\bar{H} \times \bar{f}_n^*) \cdot \hat{n}_0 \, \mathrm{d}S. \tag{6}$$

It is important to note that both sets of solenoidal and irrotational modes contribute to the EM field expansion. In particular, while for the longitudinal case [12] the solenoidal modes were sufficient, this will not be the case for the calculation of the transverse impedance.

III. DERIVATION OF THE ELECTROMAGNETIC FIELDS

The structure we study is a cavity of radius d connected with a beam pipe of radius b and filled with a toroidal insert of thickness $t = d - b$, as shown in Fig. 1. The choice of this geometry allows different accelerator devices (e.g. lossy inserts, flanges, resistive beam pipes, collimators, ferrite loaded cavities, etc.) to be modeled in an approximate way, for which either analytical formulas are available in a limited range of validity or complex finite element simulations should be envisaged. We choose a cylindrical reference system $(\hat{r}_0, \hat{\phi}_0, \hat{z}_0)$. The subdomains I and II represent the cylindrical left and right beam pipes where reflected fields propagate, III is the toroidal insert where radial waves can propagate, and IV is the cavity volume where resonances can be excited. Subdomains I, II, and IV are a vacuum (permittivity ε_0 and permeability μ_0), while III is filled with a linear, isotropic, stationary, dispersive, homogeneous material with complex relative permittivity $\varepsilon_f(\omega) = \varepsilon_f'(\omega) + j\varepsilon_f''(\omega)$, conductivity σ_c, and complex relative permeability $\mu_f(\omega) = \mu_f'(\omega) + j\mu_f''(\omega)$. The surface S_1 divides the subdomain I from IV, S_2, II from IV, S_3, and III from IV. The background is PEC (perfect electric conductor).

A. Source currents

To compute the transverse dipolar impedance, we consider, as source current, a charged particle Q displaced at $r = r_S$ traveling at velocity $v = \beta c$ along $\hat{z}_0$, with β the relativistic factor. In cylindrical coordinates, this can be written as

$$\mathcal{J}_b(r, \phi, z; t) = Qv\delta(r - r_S)\frac{\delta(\phi)}{r_S}\delta(vt - z), \tag{7}$$

where δ is the Dirac delta function and the above formula is equivalent, in frequency domain, to

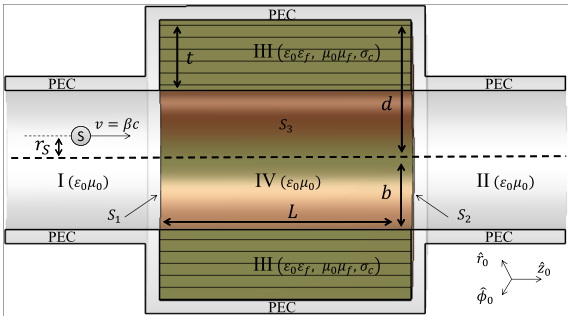

FIG. 1. Structure under study: loaded cavity connected with two beam pipes.

$$J_b(r,\phi,z;\omega) = Q\delta(r-r_S)\frac{\delta(\phi)}{r_S}e^{-j\omega z/v}. \quad (8)$$

Since we work in azimuthal symmetry, we can expand the current in Fourier series

$$J_b(r,\phi,z) = \delta(r-r_S)\sum_{m=0}^{\infty}\frac{Q\cos(m\phi)}{\pi r_S(1+\delta_{m0})}e^{-j\omega z/v}. \quad (9)$$

The term $m=1$ is a $\cos(\phi)$ modulated ring with radius r_S which will be used to calculate the dipolar impedance.

B. Source fields

In I, II, and IV, the source term is present. The solution in these subdomains can be written as the superposition of *source fields* and *scattered fields*, i.e.,

$$\bar{E}^{(\mathrm{tot})} = \bar{E}^{(\mathrm{source})} + \bar{E}^{(\mathrm{scattered})}, \quad (10)$$

$$\bar{H}^{(\mathrm{tot})} = \bar{H}^{(\mathrm{source})} + \bar{H}^{(\mathrm{scattered})}. \quad (11)$$

Since there is only one solution to the EM problem for a given beam excitation, we can choose as source fields, the ones excited by a particle beam traveling in an infinitely long perfectly conducting cylindrical beam pipe of radius b. In this way, the tangential source field continuity on S_1 and S_2 is automatically ensured, simplifying the matching operations. This approach would not be possible if the entrance beam pipe apertures would have a different shape. In that case, one could consider as source fields the ones produced by a beam traveling in vacuum. It is, by the way, also possible to formulate the mode matching problem considering directly the source current $J_b(r,\phi,z)$ in place of the source fields [14]. It is understood that the scattered fields must satisfy the source-free Maxwell equations in all the subdomains.

The source fields corresponding to the dipolar current excitation are summarized below [15]

$$E_r = -\frac{QZ_o}{\pi\beta\gamma}\frac{\alpha_b^2}{b^2\gamma}\cos(\phi)I_1(s)\frac{\partial F_1(u)}{\partial u}e^{-\frac{jz\alpha_b}{b}}, \quad (12)$$

$$E_\phi = \frac{QZ_o}{\pi\beta\gamma}\frac{\alpha_b^2}{b^2\gamma}\sin(\phi)I_1(s)\frac{F_1(u)}{u}e^{-\frac{jz\alpha_b}{b}}, \quad (13)$$

$$E_z = \frac{jQZ_o}{\pi\beta\gamma^2}\frac{\alpha_b^2}{b^2\gamma}\cos(\phi)I_1(s)F_1(u)e^{-\frac{jz\alpha_b}{b}}, \quad (14)$$

$$H_r = -\frac{Q}{\pi\gamma}\frac{\alpha_b^2}{b^2\gamma}\sin(\phi)I_1(s)\frac{F_1(u)}{u}e^{-\frac{jz\alpha_b}{b}}, \quad (15)$$

$$H_\phi = -\frac{Q}{\pi\gamma}\frac{\alpha_b^2}{b^2\gamma}\cos(\phi)I_1(s)\frac{\partial F_1(u)}{\partial u}e^{-\frac{jz\alpha_b}{b}}, \quad (16)$$

$$H_z = 0. \quad (17)$$

where

$$F_1(u) = K_1(u) - \frac{I_1(u)K_1(x)}{I_1(x)}, \quad (18)$$

with $I_\nu(u)$ and $K_\nu(u)$ representing the modified Bessel function of order ν, respectively, of first and second kind, $\alpha_b = b\omega/v$, γ the relativistic factor, $u = r\alpha_b/(b\gamma)$, $x = \alpha_b/\gamma$, and $s = r_S\omega/(\gamma v)$.

C. Scattered fields

The scattered fields for subdomains I–IV are given in Tables II–IV in Appendix A together with their relevant parameters.

For symmetry reasons, both TE and TM modes should be considered. In general, the modes propagating into the beam pipes depend on the radial mode number p and azimuthal mode number ν, the modes in the insert depend on the longitudinal mode number s and ν, the modes in the cavity depend on p, ν, and s. We consider only the scattered modes with azimuthal mode number $\nu = 1$. This is not a restriction, because, due to the azimuthal symmetry of the structure, modes with $\nu \neq 1$ do not couple with the source field and cannot be excited. From another point of view, they do not contribute to the field matching by having null projection integrals. Therefore, we suppress the ν index dependence from the field expansion.

The electric fields in the pipes and the insert (subdomains I–III) are expanded as

$$\bar{E}^{(I)} = \sum_p \mathbf{C}_\mathbf{p}^{\mathrm{TM}}\bar{E}_p^{(I,\mathrm{TM})} + \sum_p \mathbf{C}_\mathbf{p}^{\mathrm{TE}}\bar{E}_p^{(I,\mathrm{TE})}, \quad (19)$$

$$\bar{E}^{(II)} = \sum_p \mathbf{D}_\mathbf{p}^{\mathrm{TM}}\bar{E}_p^{(II,\mathrm{TM})} + \sum_p \mathbf{D}_\mathbf{p}^{\mathrm{TE}}\bar{E}_p^{(II,\mathrm{TE})}, \quad (20)$$

$$\bar{E}^{(III)} = \sum_s \mathbf{A}_\mathbf{s}^{\mathrm{TM}}\bar{E}_s^{(III,\mathrm{TM})} + \sum_s \mathbf{A}_\mathbf{s}^{\mathrm{TE}}\bar{E}_s^{(III,\mathrm{TE})}, \quad (21)$$

and analogously for the magnetic fields. In the cavity, we have

$$\bar{E}^{(IV)} = \sum_{p\,s}\mathbf{V}_{\mathbf{p}\mathbf{s}}^{\mathrm{TM}}\bar{e}_{p\,s}^{(IV,\mathrm{TM})} + \sum_{p\,s}\mathbf{V}_{\mathbf{p}\mathbf{s}}^{\mathrm{TE}}\bar{e}_{p\,s}^{(IV,\mathrm{TE})} + \sum_{p\,s}\mathbf{F}_{\mathbf{p}\mathbf{s}}\bar{f}_{p\,s}^{(IV)}, \quad (22)$$

$$\bar{H}^{(IV)} = \sum_{p\,s}\mathbf{I}_{\mathbf{p}\mathbf{s}}^{\mathrm{TM}}\bar{h}_{p\,s}^{(IV,\mathrm{TM})} + \sum_{p\,s}\mathbf{I}_{\mathbf{p}\mathbf{s}}^{\mathrm{TE}}\bar{h}_{p\,s}^{(IV,\mathrm{TE})} + \sum_{p\,s}\mathbf{G}_{\mathbf{p}\mathbf{s}}\bar{g}_{p\,s}^{(IV)}. \quad (23)$$

D. Magnetic matching

We now proceed to the matching procedure in order to find the 12 vector unknowns $\mathbf{C_p^{TM}}$, $\mathbf{D_p^{TM}}$, $\mathbf{A_s^{TM}}$, $\mathbf{I_{ps}^{TM}}$, $\mathbf{V_{ps}^{TM}}$, $\mathbf{C_p^{TE}}$, $\mathbf{D_p^{TE}}$, $\mathbf{A_s^{TE}}$, $\mathbf{I_{ps}^{TE}}$, $\mathbf{V_{ps}^{TE}}$, $\mathbf{G_{ps}}$, $\mathbf{F_{ps}}$ by means of 12 functional equations: six equations can be obtained by matching the magnetic field at the surfaces S_1, S_2 and S_3, four equations are provided by Eqs. (3) and (4) for solenoidal modes and the remaining two are provided by Eqs. (5) and (6) for the irrotational modes. Each functional equation is transformed into an infinite set of linear equations. We can immediately notice that Eq. (6) implies $\mathbf{F_{ps}} = 0$ since the irrotational electric modes $\bar{f}_{ps}$ are null on the subdomain IV boundaries. This condition does not hold for the irrotational magnetic modes.

1. Matching on S_3

Between regions III and IV, we impose the continuity of longitudinal and azimuthal magnetic field components. In the longitudinal direction, we have

$$H_z^{(III)}|_{r=b} = H_z^{(IV)}|_{r=b}. \tag{24}$$

Only the TE solenoidal and H irrotational fields have a non-null longitudinal magnetic component. Substituting the longitudinal components from Tables III and IV, and projecting over $\sin(\alpha_s z/b)$, we get

$$\mathbf{A_s^{TE}} = -\frac{\sqrt{\frac{2}{\pi}}\alpha_s}{b\mathcal{W}_{\mathrm{TEs}}(\tilde{\alpha}_{fs})}\sum_{p=1}^{\infty}\frac{\mathbf{G_{ps}}\beta_p}{\sqrt{\beta_p^2-1}\beta_{ps}} + \frac{\sqrt{\frac{2}{\pi}}}{b\mathcal{W}_{\mathrm{TEs}}(\tilde{\alpha}_{fs})}\sum_{p=1}^{\infty}\frac{\mathbf{I_{ps}^{TE}}\beta_p^2}{\sqrt{\beta_p^2-1}\beta_{ps}}. \tag{25}$$

In the azimuthal direction, we have

$$H_\phi^{(IV)}|_{r=b} + H_\phi^{(\mathrm{source})}|_{r=b} = H_\phi^{(III)}|_{r=b}. \tag{26}$$

The azimuthal components are non-null for both TE and TM fields. Substituting the field expressions from Tables II–IV and projecting over $\cos(\alpha_s z/b)$, we get

$$\sqrt{\frac{2}{\pi}}\sqrt{\frac{L}{\epsilon_s}}\frac{1}{b}\sum_{p=1}^{\infty}\frac{\mathbf{G_{ps}}\beta_p}{\sqrt{\beta_p^2-1}\beta_{ps}} + \sqrt{\frac{L}{\pi}}\frac{\alpha_s}{b}\sum_{p=1}^{\infty}\frac{\mathbf{I_{ps}^{TE}}}{\sqrt{\beta_p^2-1}\beta_{ps}} + -\sqrt{\frac{2}{\pi}}\sqrt{\frac{L}{\epsilon_s}}\frac{1}{b}\sum_{p=1}^{\infty}\mathbf{I_{ps}^{TM}} + \frac{j\alpha_b^2((-1)^s e^{-\frac{jL\alpha_b}{b}}-1)}{2\pi b\gamma(\alpha_b^2-\alpha_s^2)I_1(\frac{\alpha_b}{\gamma})} = \sqrt{\frac{L}{2}}\frac{\alpha_s\mathcal{W}_{\mathrm{TEs}}(\tilde{\alpha}_{fs})}{\tilde{\alpha}_{fs}^2}\mathbf{A_s^{TE}} - \sqrt{\frac{L}{\epsilon_s}}\frac{j\alpha_f\mathcal{W}'_{\mathrm{TMs}}(\tilde{\alpha}_{fs})}{Z_f\tilde{\alpha}_{fs}}\mathbf{A_s^{TM}}. \tag{27}$$

2. Matching on S_1

Between subdomains I and IV, we can impose the continuity of the transverse magnetic field components separately for TE and TM modes

$$\bar{H}_t^{(IV)}|_{z=0} = \bar{H}_t^{(I)}|_{z=0}. \tag{28}$$

For TM modes, projecting over $\nabla_t E_{z_q}^{(I)} \times \hat{z}_0$, we get

$$\sum_{s=0}^{\infty}\sqrt{\epsilon_s}\,\mathbf{I_{ps}^{TM}} = \frac{jb\sqrt{L}\alpha_o}{Z_o\alpha_p^2}\mathbf{C_p^{TM}}. \tag{29}$$

For TE modes, projecting over $\nabla_t H_{z_q}^{(I)}$, we get

$$\sum_{s=0}^{\infty}\frac{\alpha_s\sqrt{2}}{\beta_{ps}}\mathbf{I_{ps}^{TE}} + \sum_{s=0}^{\infty}\frac{\beta_p\sqrt{\epsilon_s}}{\beta_{ps}}\mathbf{G_{ps}} = \frac{jb\sqrt{L}\tilde{\beta}_p}{\beta_p^2}\mathbf{C_p^{TE}}. \tag{30}$$

3. Matching on S_2

Analogously, between subdomains II and IV, we have, for TM modes

$$\sum_{s=0}^{\infty}(-1)^s\sqrt{\epsilon_s}\mathbf{I_{ps}^{TM}} = \frac{jb\sqrt{L}\alpha_o}{Z_o\alpha_p^2}\mathbf{D_p^{TM}}, \tag{31}$$

and for TE modes

$$\sum_{s=0}^{\infty}\frac{\sqrt{2}(-1)^s\alpha_s}{\beta_{ps}}\mathbf{I_{ps}^{TE}} + \sum_{s=0}^{\infty}\frac{(-1)^s\beta_p\sqrt{\epsilon_s}}{\beta_{ps}}\mathbf{G_{ps}} = -\frac{jb\sqrt{L}\tilde{\beta}_p}{\beta_p^2}\mathbf{D_p^{TE}}. \tag{32}$$

E. Electric matching

According to the assumed expansion in the subdomain IV, the tangential component of the electric field on the boundary $S = S_1 \cup S_2 \cup S_3 = S_E$ is null by definition and the expansion given by Eqs. (22) and (23) does not converge uniformly on the boundaries. This difficulty is circumvented by resorting to Eqs. (3) and (4). We get the following relation between modal coefficients $\mathbf{I_{ps}}$ and $\mathbf{V_{ps}}$

$$\mathbf{I_{ps}^{TM}} = \frac{jb\alpha_o}{Z_o(\alpha_o^2-\alpha_{ps}^2)}\int_S(\bar{E}\times\bar{h}_{ps}^{*(IV,\mathrm{TM})})\cdot\hat{n}_0\mathrm{d}S, \tag{33}$$

$$\mathbf{V_{ps}^{TM}} = -\frac{jZ_o\alpha_{ps}}{\alpha_o}\mathbf{I_{ps}^{TM}}, \tag{34}$$

$$\mathbf{I_{ps}^{TE}} = \frac{jb\alpha_o}{Z_o(\alpha_o^2-\beta_{ps}^2)}\int_S(\bar{E}\times\bar{h}_{ps}^{*(IV,\mathrm{TE})})\cdot\hat{n}_0\mathrm{d}S, \tag{35}$$

$$\mathbf{V_{ps}^{TE}} = -\frac{jZ_o\beta_{ps}}{\alpha_o}\mathbf{I_{ps}^{TE}}. \tag{36}$$

The surface integral has to be split for S_1, S_2, and S_3, and after some algebra leads to

$$\mathbf{I}_{\mathbf{ps}}^{\mathrm{TM}} = \frac{jb\alpha_o}{Z_o(\alpha_o^2-\alpha_{ps}^2)}\left(\frac{jb\tilde{\alpha}_p}{\alpha_p^2}\sqrt{\frac{\epsilon_s}{L}}\mathbf{C}_{\mathbf{p}}^{\mathrm{TM}} + \frac{jb\tilde{\alpha}_p}{\alpha_p^2}(-1)^s\sqrt{\frac{\epsilon_s}{L}}\mathbf{D}_{\mathbf{p}}^{\mathrm{TM}} + \sqrt{2\pi}\mathcal{W}_{\mathrm{TMs}}(\tilde{\alpha}_{fs})\mathbf{A}_{\mathbf{s}}^{\mathrm{TM}}\right), \tag{37}$$

and

$$\mathbf{I}_{\mathbf{ps}}^{\mathrm{TE}} = \frac{jb\alpha_o}{Z_o(\alpha_o^2-\beta_{ps}^2)}\left(\frac{jb\alpha_o\alpha_s}{Y_0\beta_p^2\beta_{ps}}\sqrt{\frac{2}{L}}\mathbf{C}_{\mathbf{p}}^{\mathrm{TE}} - \frac{jb\alpha_o\alpha_s}{Y_0\beta_p^2\beta_{ps}}\sqrt{\frac{2}{L}}(-1)^s\mathbf{D}_{\mathbf{p}}^{\mathrm{TE}} + -\frac{j\sqrt{2\pi}\alpha_f\beta_p^2(\delta_{s0}-1)\mathcal{W}'_{\mathrm{TEs}}(\tilde{\alpha}_{fs})}{Y_f\sqrt{\beta_p^2-1}\beta_{ps}\tilde{\alpha}_{fs}}\mathbf{A}_{\mathbf{s}}^{\mathrm{TE}} - \frac{\sqrt{\pi}\alpha_s\sqrt{\epsilon_s}(\alpha_f^2-\beta_{ps}^2)\mathcal{W}_{\mathrm{TMs}}(\tilde{\alpha}_{fs})}{\sqrt{\beta_p^2-1}\beta_{ps}\tilde{\alpha}_{fs}^2}\mathbf{A}_{\mathbf{s}}^{\mathrm{TM}}\right). \tag{38}$$

The $\mathbf{G}_{\mathbf{ps}}$ coefficients of the irrotational modes H can be derived from Eq. (5) which, in this context, may be rewritten as

$$\mathbf{G}_{\mathbf{ps}} = \frac{jbY_0}{\alpha_o}\int_S (\bar{E}\times\bar{g}_{ps}^*)\cdot\hat{n}_0\,\mathrm{d}S. \tag{39}$$

Solving the integral, we have

$$\mathbf{G}_{\mathbf{ps}} = \frac{jbY_0}{\alpha_o} \times\left(-\frac{\sqrt{\frac{\pi}{2}}\beta_p\epsilon_s((\delta_{s0}+1)\tilde{\alpha}_{fs}^2+\alpha_s^2)\mathcal{W}_{\mathrm{TMs}}(\tilde{\alpha}_{fs})}{\sqrt{\beta_p^2-1}\beta_{ps}\tilde{\alpha}_{fs}^2}\mathbf{A}_{\mathbf{s}}^{\mathrm{TM}} - \frac{j\sqrt{\pi}\alpha_f\beta_p\alpha_s\sqrt{\epsilon_s}\mathcal{W}'_{\mathrm{TEs}}(\tilde{\alpha}_{fs})}{Y_f\sqrt{\beta_p^2-1}\beta_{ps}\tilde{\alpha}_{fs}}\mathbf{A}_{\mathbf{s}}^{\mathrm{TE}} + \frac{jb\alpha_o}{Y_0\beta_p\beta_{ps}}\sqrt{\frac{\epsilon_s}{L}}\mathbf{C}_{\mathbf{p}}^{\mathrm{TE}} - \frac{jb(-1)^s\alpha_o}{Y_0\beta_p\beta_{ps}}\sqrt{\frac{\epsilon_s}{L}}\mathbf{C}_{\mathbf{p}}^{\mathrm{TE}}\right). \tag{40}$$

Up to this point, we collected nine independent relations given by Eqs. (25), (27), (29), (30)–(32), (37), (38), and (40) in nine variables, $\mathbf{C}_{\mathbf{p}}^{\mathrm{TM}}$, $\mathbf{D}_{\mathbf{p}}^{\mathrm{TM}}$, $\mathbf{A}_{\mathbf{s}}^{\mathrm{TM}}$, $\mathbf{I}_{\mathbf{ps}}^{\mathrm{TM}}$, $\mathbf{C}_{\mathbf{p}}^{\mathrm{TE}}$, $\mathbf{D}_{\mathbf{p}}^{\mathrm{TE}}$, $\mathbf{A}_{\mathbf{s}}^{\mathrm{TE}}$, $\mathbf{I}_{\mathbf{ps}}^{\mathrm{TE}}$, $\mathbf{G}_{\mathbf{ps}}$. The $\mathbf{V}_{\mathbf{ps}}^{\mathrm{TM}}$ coefficients are linearly related to the $\mathbf{I}_{\mathbf{ps}}^{\mathrm{TM}}$ with Eq. (34) and similarly for the $\mathbf{V}_{\mathbf{ps}}^{\mathrm{TE}}$ ones.

F. Sum manipulation

In order to simplify the numerical implementation of the equations, some series can be closed. In the following, we will use the results summarized in Appendix B.

Inserting Eq. (37) in Eq. (29) and summing over the s index with Eqs. (B1) and (B2), we get

$$\mathbf{C}_{\mathbf{p}}^{\mathrm{TM}}\left(\cot\left(\frac{L\tilde{\alpha}_p}{b}\right)+j\right) + \mathbf{D}_{\mathbf{p}}^{\mathrm{TM}}\csc\left(\frac{L\tilde{\alpha}_p}{b}\right) = j\sqrt{\frac{2\pi}{L}}\alpha_p^2\sum_{s=0}^{\infty}\frac{\sqrt{\epsilon_s}\mathcal{W}_{\mathrm{TMs}}(\tilde{\alpha}_{fs})}{\alpha_o^2-\alpha_{ps}^2}\mathbf{A}_{\mathbf{s}}^{\mathrm{TM}}. \tag{41}$$

In a similar way, inserting Eq. (37) in Eq. (31), we get

$$\mathbf{C}_{\mathbf{p}}^{\mathrm{TM}}\csc\left(\frac{L\tilde{\alpha}_p}{b}\right) + \mathbf{D}_{\mathbf{p}}^{\mathrm{TM}}\left(\cot\left(\frac{L\tilde{\alpha}_p}{b}\right)+j\right) = j\sqrt{\frac{2\pi}{L}}\alpha_p^2\sum_{s=0}^{\infty}\frac{(-1)^s\sqrt{\epsilon_s}\mathcal{W}_{\mathrm{TMs}}(\tilde{\alpha}_{fs})}{\alpha_o^2-\alpha_{ps}^2}\mathbf{A}_{\mathbf{s}}^{\mathrm{TM}}. \tag{42}$$

Solving the system in the two variables $\mathbf{C}_{\mathbf{p}}^{\mathrm{TM}}$ and $\mathbf{D}_{\mathbf{p}}^{\mathrm{TM}}$ and passing to a matrix representation, we have

$$\mathbf{C}_{\mathbf{P\times 1}}^{\mathrm{TM}} = \mathrm{N1}_{P\times P}\cdot\mathrm{M1}_{P\times S}\cdot\mathbf{A}_{\mathbf{S\times 1}}^{\mathrm{TM}}, \tag{43}$$

$$\mathbf{D}_{\mathbf{P\times 1}}^{\mathrm{TM}} = \mathrm{N1}_{P\times P}\cdot\mathrm{M1}_{P\times S}\cdot\mathrm{II}_{S\times S}\cdot\mathbf{A}_{\mathbf{S\times 1}}^{\mathrm{TM}}, \tag{44}$$

with matrix elements reported in Eqs. (C1)–(C3) of Appendix C.

Another system can be obtained by inserting Eqs. (38) and (40), respectively, in Eqs. (30) and (32). Summing over the s index with Eqs. (B3)–(B6), we get

$$\mathbf{C}_{\mathbf{P\times 1}}^{\mathrm{TE}} = \mathrm{N2}_{P\times P}\cdot\mathrm{M2}_{P\times S}\cdot\mathbf{A}_{\mathbf{S\times 1}}^{\mathrm{TE}} + \mathrm{N2}_{P\times P}\cdot\mathrm{M3}_{P\times S}\cdot\mathbf{A}_{\mathbf{S\times 1}}^{\mathrm{TM}}, \tag{45}$$

$$\mathbf{D}_{\mathbf{P\times 1}}^{\mathrm{TE}} = \mathrm{N2}_{P\times P}\cdot\mathrm{M2}_{P\times S}\cdot\mathrm{II}_{S\times S}\cdot\mathbf{A}_{\mathbf{S\times 1}}^{\mathrm{TE}} + \mathrm{N2}_{P\times P}\cdot\mathrm{M3}_{P\times S}\cdot\mathrm{II}_{S\times S}\cdot\mathbf{A}_{\mathbf{S\times 1}}^{\mathrm{TM}}, \tag{46}$$

with matrix elements reported in Eqs. (C4)–(C6).

Inserting Eqs. (37), (38), and (40) in Eq. (27) and summing over the index p making use of Eqs. (B13)–(B17), we get

$$\begin{aligned}&\mathrm{B}_{S\times 1} + \mathrm{F1}_{S\times S}\cdot\mathbf{A}_{\mathbf{S\times 1}}^{\mathrm{TE}} + \mathrm{F2}_{S\times S}\cdot\mathbf{A}_{\mathbf{S\times 1}}^{\mathrm{TM}}\\ &- (\mathrm{T1}_{S\times S}\cdot\mathrm{G1}_{S\times P} + \mathrm{T2}_{S\times S}\cdot\mathrm{G2}_{S\times P})\cdot\mathbf{C}_{\mathbf{P\times 1}}^{\mathrm{TE}}\\ &+ \mathrm{II}_{S\times S}\cdot(\mathrm{T1}_{S\times S}\cdot\mathrm{G1}_{S\times P} + \mathrm{T2}_{S\times S}\cdot\mathrm{G2}_{S\times P})\cdot\mathbf{D}_{\mathbf{P\times 1}}^{\mathrm{TE}}\\ &+ \mathrm{T3}_{S\times S}\cdot\mathrm{G3}_{S\times P}\cdot\mathbf{C}_{\mathbf{P\times 1}}^{\mathrm{TM}}\\ &+ \mathrm{II}_{S\times S}\cdot\mathrm{T3}_{S\times S}\cdot\mathrm{G3}_{S\times P}\cdot\mathbf{D}_{\mathbf{P\times 1}}^{\mathrm{TM}} = 0,\end{aligned} \tag{47}$$

and the matrix elements are reported in Eqs. (C7)–(C15).

Inserting Eqs. (38) and (40) in Eq. (25) making use of Eqs. (B14) and (B17)–(B19), we get

$$\begin{aligned}&\mathrm{F3}_{S\times S}\cdot\mathbf{A}^{\mathrm{TE}}_{\mathbf{S\times 1}}+\mathrm{F4}_{S\times S}\cdot\mathbf{A}^{\mathrm{TM}}_{\mathbf{S\times 1}}\\&\quad-(\mathrm{T4}_{S\times S}\cdot\mathrm{G4}_{S\times P}-\mathrm{T5}_{S\times S}\cdot\mathrm{G5}_{S\times P})\cdot\mathbf{C}^{\mathrm{TE}}_{\mathbf{P\times 1}}\\&\quad+\mathrm{II}_{S\times S}\cdot(\mathrm{T4}_{S\times S}\cdot\mathrm{G4}_{S\times P}-\mathrm{T5}_{S\times S}\cdot\mathrm{G5}_{S\times P})\cdot\mathbf{D}^{\mathrm{TE}}_{\mathbf{P\times 1}}=0,\end{aligned}\tag{48}$$

where the matrix elements are reported in Eqs. (C16)–(C21).

Recapitulating the matching equations, we have six vector equations in six independent vector variables, the problem is formally solved and the coefficients $\mathbf{C}^{\mathrm{TM}}_{\mathbf{P\times 1}}$, $\mathbf{D}^{\mathrm{TM}}_{\mathbf{P\times 1}}$, $\mathbf{C}^{\mathrm{TE}}_{\mathbf{P\times 1}}$, $\mathbf{D}^{\mathrm{TE}}_{\mathbf{P\times 1}}$, $\mathbf{A}^{\mathrm{TM}}_{\mathbf{S\times 1}}$, and $\mathbf{A}^{\mathrm{TE}}_{\mathbf{S\times 1}}$ can be now found with a numerical inversion of the truncated matrices.

G. Impedance calculation

The transverse dipolar impedance can be calculated dividing the calculation for the three subdomains I, II, and IV. From now on, we consider a small source displacement, i.e., $r_S\to 0$, so that we can simplify the source matrix $\mathrm{B}_{S\times 1}$ of Eq. (47) with $I_1(s)/r_S\to 1/2$. In subdomain I, we have

$$\begin{aligned}Z^{(I)}_{\mathrm{dip}}(\omega)=&\,j\int_{-\infty}^{0}\mathrm{d}z\,e^{j\alpha_b z/b}\sum_{p=1}^{\infty}\mathbf{C}^{\mathrm{TM}}_{\mathbf{p}}(E^{(I,\mathrm{TM})}_{r_p}-\beta c\mu_0 H^{(I,\mathrm{TM})}_{\phi_p})\\&+j\int_{-\infty}^{0}\mathrm{d}z e^{j\alpha_b z/b}\sum_{p=1}^{\infty}\mathbf{C}^{\mathrm{TE}}_{\mathbf{p}}(E^{(I,\mathrm{TE})}_{r_p}-\beta c\mu_0 H^{(I,\mathrm{TE})}_{\phi_p}).\end{aligned}$$

Substituting the field components from Tables II and III and integrating, we get

$$\begin{aligned}Z^{(I)}_{\mathrm{dip}}(\omega)=&\sum_{p=1}^{\infty}\frac{jb\mathbf{C}^{\mathrm{TM}}_{\mathbf{p}}(\tilde{\alpha}_p+\beta\alpha_o)}{\sqrt{2\pi}\alpha_p^2J_0(\alpha_p)(\tilde{\alpha}_p+\alpha_b)}\\&+\sum_{p=1}^{\infty}\frac{-jb\mathbf{C}^{\mathrm{TE}}_{\mathbf{p}}(\beta\tilde{\beta}_p+\alpha_o)}{\sqrt{2\pi}Y_o\beta_p^2\sqrt{\beta_p^2-1}J_0(\beta_p)(\tilde{\beta}_p+\alpha_b)}.\end{aligned}\tag{49}$$

Analogously, we can do this for subdomain II obtaining

$$\begin{aligned}Z^{(II)}_{\mathrm{dip}}(\omega)=&\sum_{p=1}^{\infty}\frac{-jb\mathbf{D}^{\mathrm{TM}}_{\mathbf{p}}e^{\frac{jL\alpha_b}{b}}(\beta\alpha_o-\tilde{\alpha}_p)}{\sqrt{2\pi}\alpha_p^2J_0(\alpha_p)(\alpha_b-\tilde{\alpha}_p)}\\&+\sum_{p=1}^{\infty}\frac{jb\mathbf{D}^{\mathrm{TE}}_{\mathbf{p}}e^{\frac{jL\alpha_b}{b}}(\alpha_o-\beta\tilde{\beta}_p)}{\sqrt{2\pi}Y_o\beta_p^2\sqrt{\beta_p^2-1}J_0(\beta_p)(\alpha_b-\tilde{\beta}_p)}.\end{aligned}\tag{50}$$

Truncating at $p_{\max}=P$ radial modes, we have

$$Z^{(I)}_{\mathrm{dip}}=Z^{C_{\mathrm{TM}}}_{1\times P}\cdot\mathbf{C}^{\mathrm{TM}}_{\mathbf{P\times 1}}+Z^{C_{\mathrm{TE}}}_{1\times P}\cdot\mathbf{C}^{\mathrm{TE}}_{\mathbf{P\times 1}},\tag{51}$$

$$Z^{(II)}_{\mathrm{dip}}=Z^{D_{\mathrm{TM}}}_{1\times P}\cdot\mathbf{D}^{\mathrm{TM}}_{\mathbf{P\times 1}}+Z^{D_{\mathrm{TE}}}_{1\times P}\cdot\mathbf{D}^{\mathrm{TE}}_{\mathbf{P\times 1}},\tag{52}$$

with matrix elements reported in Eqs. (D1)–(D4) of Appendix D.

In cavity subdomain IV, the fields are given by Eqs. (22) and (23). We consider separately the contribution of TM, TE, and irrotational modes to the impedance. Starting from the TM contribution, we have

$$\begin{aligned}&Z^{(IV_{\mathrm{TM}})}_{\mathrm{dip}}(\omega)\\&=\sum_{p\,s}^{\infty}j\int_0^L\mathrm{d}z e^{j\alpha_b z/b}(\mathbf{V}^{\mathrm{TM}}_{\mathbf{ps}}e^{(IV,\mathrm{TM})}_{r_{ps}}-\beta Z_o\mathbf{I}^{\mathrm{TM}}_{\mathbf{ps}}h^{(IV,\mathrm{TM})}_{\phi_{ps}}).\end{aligned}$$

To solve this expression, we can write the coefficients $\mathbf{V}^{\mathrm{TM}}_{\mathbf{ps}}$ as function of $\mathbf{I}^{\mathrm{TM}}_{\mathbf{ps}}$ resorting to Eq. (34) and substitute the $\mathbf{I}^{\mathrm{TM}}_{\mathbf{ps}}$ by means of Eq. (37) in order to recollect the known coefficients $\mathbf{C}^{\mathrm{TM}}_{\mathbf{p}}$, $\mathbf{D}^{\mathrm{TM}}_{\mathbf{p}}$, and $\mathbf{A}^{\mathrm{TM}}_{\mathbf{s}}$. Substituting the field expressions from Table IV and summing over p and s indices with the help of Eqs. (B20), (B7), and (B8), we get

$$\begin{aligned}Z^{(IV_{\mathrm{TM}})}_{\mathrm{dip}}=&\,Z^{IV_{\mathrm{TM}},C_{\mathrm{TM}}}_{1\times P}\cdot\mathbf{C}^{\mathrm{TM}}_{\mathbf{P\times 1}}+Z^{IV_{\mathrm{TM}},D_{\mathrm{TM}}}_{1\times P}\cdot\mathbf{D}^{\mathrm{TM}}_{\mathbf{P\times 1}}\\&+Z^{IV_{\mathrm{TM}},A_{\mathrm{TM}}}_{1\times S}\cdot\mathbf{A}^{\mathrm{TM}}_{\mathbf{S\times 1}},\end{aligned}$$

where we truncated the matrices at $p_{\max}=P$ and $s_{\max}=S$. The matrix elements are reported in Eqs. (D5)–(D6).

In a similar way, we can derive the TE contribution

$$\begin{aligned}&Z^{(IV_{\mathrm{TE}})}_{\mathrm{dip}}(\omega)\\&=\sum_{p\,s}^{\infty}j\int_0^L\mathrm{d}z\,e^{j\alpha_b z/b}(\mathbf{V}^{\mathrm{TE}}_{\mathbf{ps}}e^{(IV,\mathrm{TE})}_{r_{ps}}-\beta Z_o\mathbf{I}^{\mathrm{TE}}_{\mathbf{ps}}h^{(IV,\mathrm{TE})}_{\phi_{ps}}).\end{aligned}$$

The $\mathbf{V}^{\mathrm{TE}}_{\mathbf{ps}}$ coefficients can be expressed in function of $\mathbf{I}^{\mathrm{TE}}_{\mathbf{ps}}$ resorting to Eq. (36) and we can substitute the $\mathbf{I}^{\mathrm{TE}}_{\mathbf{ps}}$ by means of Eq. (38) and the known coefficients $\mathbf{C}^{\mathrm{TE}}_{\mathbf{p}}$, $\mathbf{D}^{\mathrm{TE}}_{\mathbf{p}}$, $\mathbf{A}^{\mathrm{TM}}_{\mathbf{s}}$, and $\mathbf{A}^{\mathrm{TE}}_{\mathbf{s}}$. We get

$$\begin{aligned}Z^{(IV_{\mathrm{TE}})}_{\mathrm{dip}}=&\,Z^{IV_{\mathrm{TE}},C_{\mathrm{TE}}}_{1\times P}\cdot\mathbf{C}^{\mathrm{TE}}_{\mathbf{P\times 1}}+Z^{IV_{\mathrm{TE}},D_{\mathrm{TE}}}_{1\times P}\cdot\mathbf{D}^{\mathrm{TE}}_{\mathbf{P\times 1}}\\&+Z^{IV_{\mathrm{TE}},A_{\mathrm{TM}}}_{1\times S}\cdot\mathbf{A}^{\mathrm{TM}}_{\mathbf{S\times 1}}+Z^{IV_{\mathrm{TE}},A_{\mathrm{TE}}}_{1\times S}\cdot\mathbf{A}^{\mathrm{TE}}_{\mathbf{S\times 1}}.\end{aligned}$$

It is interesting to notice the presence of the term $\mathbf{A}^{\mathrm{TM}}_{\mathbf{s}}$ which couples in the impedance the effect of both TE and TM modes. Substituting the field expressions and summing over the p and s index using Eqs. (B21), (B22), (B9), and (B10), we get Eqs. (D8)–(D11).

The last impedance term is the one coming from the irrotational modes. Since we found $\mathbf{F_{ps}} = 0$, we calculate only the contribution from the modes H, i.e., involving the $\mathbf{G_{ps}}$ coefficients. We have

$$Z_{\mathrm{dip}}^{(IV_H)}(\omega) = \sum_{p\,s}^{\infty} j \int_0^L \mathrm{d}z\, e^{j\alpha_b z/b}(-\beta Z_o \mathbf{G_{ps}} g_{\phi_{ps}}).$$

Inserting Eq. (40), we can write $\mathbf{G_{ps}}$ as a function of the known coefficients $\mathbf{C_p^{TE}}$, $\mathbf{D_p^{TE}}$, $\mathbf{A_s^{TM}}$, and $\mathbf{A_s^{TE}}$ and obtain

$$Z_{\mathrm{dip}}^{(IV_H)} = Z_{1\times P}^{IV_H, C_{\mathrm{TE}}} \cdot \mathbf{C_{P\times 1}^{TE}} + Z_{1\times P}^{IV_H, D_{\mathrm{TE}}} \cdot \mathbf{D_{P\times 1}^{TE}} + Z_{1\times S}^{IV_H, A_{\mathrm{TM}}} \cdot \mathbf{A_{S\times 1}^{TM}} + Z_{1\times S}^{IV_H, A_{\mathrm{TE}}} \cdot \mathbf{A_{S\times 1}^{TE}}.$$

Substituting the field expressions and summing over the p and s index using Eqs. (B21), (B11), and (B12), we get Eqs. (D12)–(D15).

The impedance can therefore be written as

$$Z_{\mathrm{dip}}(\omega) = Z_{\mathrm{dip}}^{(I)}(\omega) + Z_{\mathrm{dip}}^{(II)}(\omega) + Z_{\mathrm{dip}}^{(IV_{\mathrm{TM}})}(\omega) + Z_{\mathrm{dip}}^{(IV_{\mathrm{TE}})}(\omega) + Z_{\mathrm{dip}}^{(IV_H)}(\omega). \tag{53}$$

As we anticipated in Sec. II, and contrary to the longitudinal impedance case studied in [12], Eq. (53) also shows a contribution from the irrotational modes.

IV. APPLICATIONS

In this section, we show a series of studies related to the impedance dependence on the conductivity σ of the material in region III, on the length L of the device, and on the velocity v of the particle beam. The model dimensions are, unless differently specified, $b = 5$ cm, $t = 25$ cm, and $L = 20$ cm according to Fig. 1. The material filling region III has the properties $\varepsilon_d = \varepsilon_0 - j\sigma_c/\omega$, $\mu_d = \mu_0$.

First, we will show the convergence of the method as a function of the number of simulated cavity modes (IV A), then resonant frequencies (IV B), and the low frequency impedance in an empty cavity (IV C). We will then consider the case of a conductive insert (IV D) with a detailed analysis of related trapped modes (IV E). We conclude by showing the impedance dependence on beam velocity (IV F).

A. Convergence

Depending on the case under study, the convergence of the mode matching depends on the number of longitudinal S modes and radial P modes used in the matrix computation. We defined S and P as the maximum number of longitudinal and radial cavity modes, with s and p the longitudinal and radial mode indices. Once S and P are fixed, the modal index is $p \in (1, \ldots, P)$ and $s \in (0, \ldots, S-1)$ for TM modes and $s \in (1, \ldots, S)$ for TE modes. This is also the convention in the MATLAB [16] code we implemented. Given the geometry (in terms of beam pipe radius b, cavity thickness t, and insert length L), we can estimate the maximum number of modes P and S needed in order to reach the maximum frequency f_{max} we are interested in.

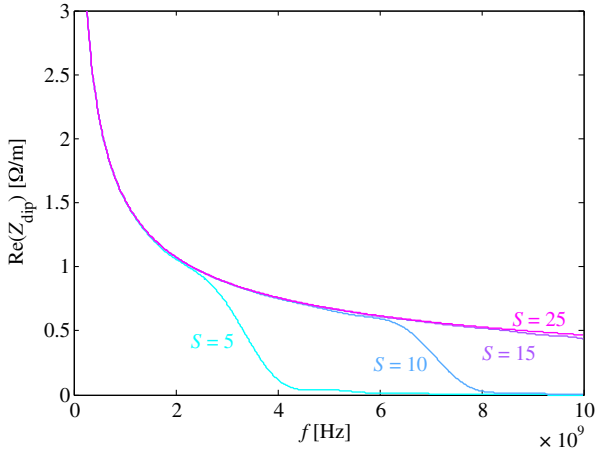

FIG. 2. Convergence of mode matching as a function of the number of longitudinal modes S. Mode matching parameters: $b = 5$ cm, $t = 25$ cm, $L = 20$ cm, $\sigma_c = 10^6$ S/m, $\beta = 1$.

Figure 2 shows the impedance calculation for the case of a resistive insert with $\sigma_c = 10^6$ S/m. Different choices of S are shown ($S = 5, 10, 15, 25$) for the same number of radial modes ($P = 5$). In the case of $S = 25$, we reach convergence in the frequency span from 0 to 10 GHz, the region of typical interest in accelerator physics applications. If instead, we consider the case $S = 5$, $P = 5$, the maximum frequency f_{max} that could be simulated is 3.8 GHz. The number of radial modes P is less relevant since the current flows mainly on the insert surface and therefore radial resonances are not expected.

For low conductivity, resonant modes start to appear and the role of P modes becomes evident. Figure 3 shows the case for a very narrow empty cavity ($\sigma_c = 10^{-10}$ S/m). In this case, $S = 1$ is sufficient to cover the frequency range of interest while, due to the thickness, we have to consider $P = 20$ in order to obtain a reasonable convergence. The frequency is normalized over the first beam pipe propagating mode (TE_{11}), known as cutoff frequency, defined as

$$f_{co}^{\mathrm{TE}} = \beta_{1,1}\frac{c}{b}, \tag{54}$$

where $\beta_{1,1} \simeq 1.8411$ is the eigenvalue corresponding to the TE_{11} propagating mode. We let the reader notice, that convergence is reached regardless the ratio of S/P. This is sometimes required in other studies involving a truncation of a doubly infinite set of equations [17].

B. Empty cavity: Mode excitation

The TM and TE modes in an empty cavity are given by (see, for example [13])

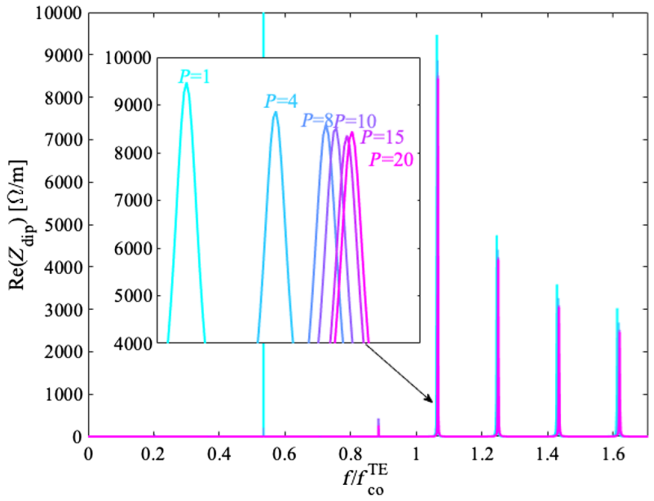

FIG. 3. Convergence of mode matching as a function of the number of radial modes P. Frequency is normalized over the first beam pipe propagating mode (TE_{11}). Mode matching parameters: $b = 5$ cm, $t = 45$ cm, $L = 2$ mm, $\sigma_c = 10^{-10}$ S/m, $\beta = 1$.

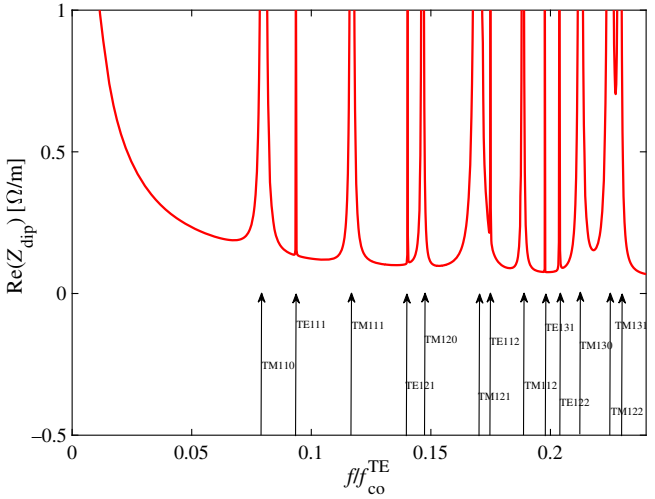

FIG. 4. TM and TE modes excited in the dipolar impedance. Frequency is normalized over the first beam pipe propagating mode (TE_{11}). Mode matching parameters: $b = 1$ cm, $t = 25$ cm, $L = 20$ cm, $\sigma_c = 10^{-7}$ S/m, $\beta = 1$, $P = 10$, $S = 10$.

$$f^{\mathrm{TM}}_{1,p,s} = \frac{c}{2\pi b}\sqrt{\alpha^2_{1,p} + \alpha^2_s}, \quad \text{with s} \in (0, 1, \ldots) \quad \text{and} \quad \text{p} \in (1, 2, \ldots), \tag{55}$$

$$f^{\mathrm{TE}}_{1,p,s} = \frac{c}{2\pi b}\sqrt{\beta^2_{1,p} + \alpha^2_s}, \quad \text{with s} \in (1, 2, \ldots) \quad \text{and} \quad \text{p} \in (1, 2, \ldots), \tag{56}$$

where we restricted ourselves to the dipole modes. In order to compare the mode frequency from theory and mode matching implementation, we choose a small beam pipe radius with respect to the cavity thickness ($b = 1$ cm and $t = 25$ cm): in this way, we can push the beam pipe cutoff frequency f^{TE}_{co} well above the first cavity resonant mode avoiding the resonant frequency shift due to the coupling with the beam pipes. The conductivity σ_c, moreover, has been set to $\sigma_c = 10^{-7}$ S/m in order to be able to appreciate the resonant shape in the real part of the impedance (a null conductivity would give rise to Dirac functions at resonant frequencies). Figure 4 shows the real part of the transverse dipolar impedance. Arrows are placed at the frequencies calculated with Eqs. (55) and (56). A good agreement for the resonant frequency location is observed between these predictions and the mode matching modes. We note that, even if the beam represents a TM-like excitation (there is no magnetic field component in the z direction), the TE modes are anyway excited. The slow impedance growth toward low frequencies is due to the fact that we had to choose a small, but nonzero, conductivity σ_c in order to make the modes visible: this does not in any way affect the mode location whose frequency implies $\omega\varepsilon_0 \gg \sigma_c$.

C. Empty cavity: Low frequency impedance

The impedance of an empty cavity at low frequency represents a classical problem already analyzed by other authors. In particular, here, we compare the mode matching transverse impedance with formulas given in [18] for the low frequency regime. The impedance at low frequency is

$$Z^{\text{low freq}}_{\text{dip}} = -j\frac{Z_0 L}{\pi b^2}\frac{S^2 - 1}{S^2 + 1}, \tag{57}$$

valid for $L < \pi^2 \frac{b}{32}$ [19] and $f < f_{\mathrm{TM}_{010}}$ with $S = (b + t)/b$. Figure 5 shows the convergence to the theoretical value for small cavity length. With $L < 0.001$, the condition $L < \pi^2 \frac{b}{32}$ is fulfilled within 6% and mode matching and theory

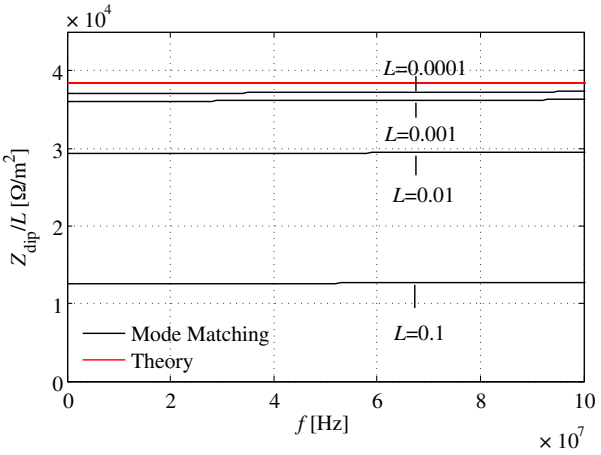

FIG. 5. Comparison of mode matching with the classical low frequency impedance in an empty cavity [18]. Mode matching parameters: $b = 5$ cm, $t = 10$ cm, $L \in (10^{-4}, \ldots, 0.1)$ m, $\sigma_c = 10^{-12}$ S/m, $\beta = 1$.

are closer. We observe that, outside of the range of applicability of the analytical formula, the low frequency impedance does not scale linearly with the insert length.

D. Conductive insert: Benchmark on length, thickness, and conductivity

We introduce two frequency parameters f_c and f_{skin}. The parameter f_c is the frequency limit at which a metal with a given conductivity σ_c can be treated as a good conductor ($\sigma_c > \omega\varepsilon_0$) and is defined as

$$f_c = \frac{\sigma_c}{2\pi\varepsilon_0}. \tag{58}$$

The parameter f_{skin} is the frequency at which the skin depth $\delta_{\mathrm{skin}} = \sqrt{2/(\omega\mu\sigma_c)}$ equals the insert thickness t. It is important to notice that we can define f_{skin} only in the hypothesis of good conductor, i.e., $\sigma_c > \omega\varepsilon_0$ or $f < f_c$.

1. Case $f < f_c$ and $t < b$, $L > b$

For long devices and thin conducting layers, the resistive wall theory can be applied in both low frequency regime (LF, valid for $f < f_{\mathrm{skin}}$) and intermediate frequency regime (IF, valid for $f > f_{\mathrm{skin}}$) [18,20]. The classical resistive wall formulas in these regimes are

$$Z_{\mathrm{dip}}^{LF} = \frac{jZ_o t}{\pi b^3} L, \tag{59}$$

$$Z_{\mathrm{dip}}^{IF} = \frac{\beta c}{\omega}\frac{1+j}{\pi\sigma_c\delta_{\mathrm{skin}}b^3} L. \tag{60}$$

Figure 6 shows the comparison between mode matching and the classical theory of resistive wall impedance: the agreement is good within a wide range of frequencies in both LF and IF regimes.

2. Case $f < f_c$ and $t > b$

In case the thickness becomes comparable or larger than the beam pipe radius (e.g., in collimators), the LF resistive wall formula does not hold anymore since it assumes $t \ll b$. In order to cover this range of frequencies, we can compare our model with IW2D [21], a 2D code based on field matching to study the impedance of multilayer beam pipes of flat and circular cross sections. It is important to note that IW2D does not implement PEC layers. In order to simulate our boundary condition, we therefore chose an ideally highly conductive material with $\sigma_c = 10^{10}$ S/m and infinite thickness.

Figure 7 shows the impedance normalized over the cavity length. The normalization is performed as IW2D is developed within the *infinite length* approximation. When $L < b$, the transverse LF impedance in the mode matching model becomes higher by up to a factor 2 with respect to IW2D [see Fig. 7 (bottom)]. This effect becomes apparent only for short inserts at very low frequencies (10–100 Hz) and it is related to the increased insert capacitance.

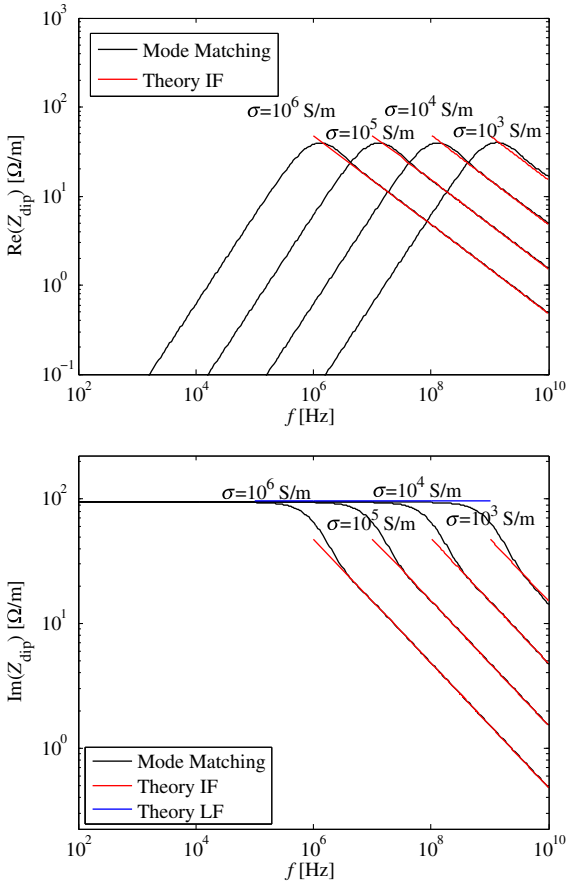

FIG. 6. Comparison between mode matching and the classical theory of resistive wall of [18,20] real and imaginary part of the transverse impedance. Mode matching parameters: $b = 5$ cm, $t = 500$ μm, $L = 20$ cm, $\sigma_c \in (10^3, \ldots, 10^6)$ S/m, $\beta = 1$, $P = 10$, $S = 20$.

3. Case $f > f_c$ and $L > b$, $t > b$

To complete our treatment, we consider the case of elongated structures with low conductivity, i.e., $\sigma_c \in (10^{-5}, \ldots, 10^5)$ S/m for which cavity resonances start to play a role and analytical formulas are not available. The low conductivity could represent effective dielectric losses characterized by the material loss tangent $\tan\delta$ for which $\sigma_{c,\mathrm{eq}} = \omega\varepsilon_0\varepsilon_r \tan\delta$ (e.g., ceramic chambers). To prove the validity of our method also in this case, we can benchmark it with the Wakefield solver of a commercial particle simulation tool, CST Studio Suite® by Dassault Systèmes [22]. CST is a time domain code in which a truncated Gaussian particle distribution $\rho(s)$ can be tracked along the device under test. The bunch length settles the maximum simulated frequency.

Figure 8 shows the mode matching benchmark with CST for $\sigma_c = 10^{-2}$ S/m and with a bunch length $\sigma_b = 2$ cm where a good agreement has been achieved.

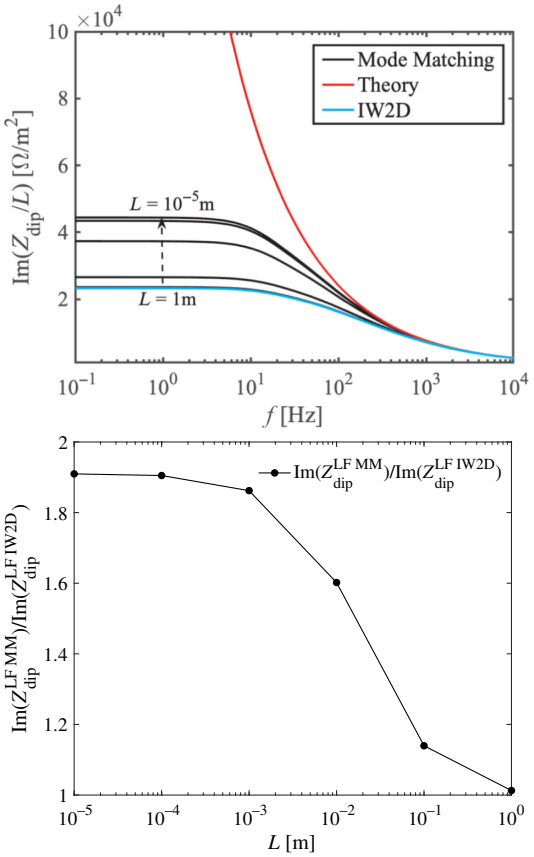

FIG. 7. Imaginary part of the dipolar impedance from the mode matching and IW2D model normalized by the cavity length (top) and ratio in the LF regime (bottom). Mode matching parameters: $b = 5$ cm, $t = 25$ cm, $\sigma_c = 10^6$ S/m, $\beta = 1$, $P = 10$, $S = 10$.

E. Trapped modes

An interesting effect, relevant for short inserts with low conductivity, is the presence of trapped modes below the beam pipe cutoff frequencies, which could be of interest in the frame of beam stability studies. In the longitudinal plane, this effect was studied close to the TM_{01} cutoff and it was characterized by a transmission line model with lumped parameters. While the same effect appears also on the dipolar impedance, close to the TE cutoff frequencies, a similar model is not easily applicable. Figure 9, on the top, shows the dipolar impedance perturbed by a trapped mode slightly below cutoff. We may note that at exactly the cutoff frequency, i.e., $f/f^{\mathrm{TE}}_{co} = 1$, the impedance appears unperturbed, as shown in the bottom plot.

The trapped mode frequency shift relative to the TE_{11} cutoff frequency has been evaluated for small discontinuities by different authors [23,24]. Here, we compare the perturbation theory developed in [24] to the trapped mode frequency shift calculated with the mode matching and CST simulations. Figure 10 shows the comparison between the three different methods as a function of the ratio t/b of the cavity. While there is agreement between the perturbative

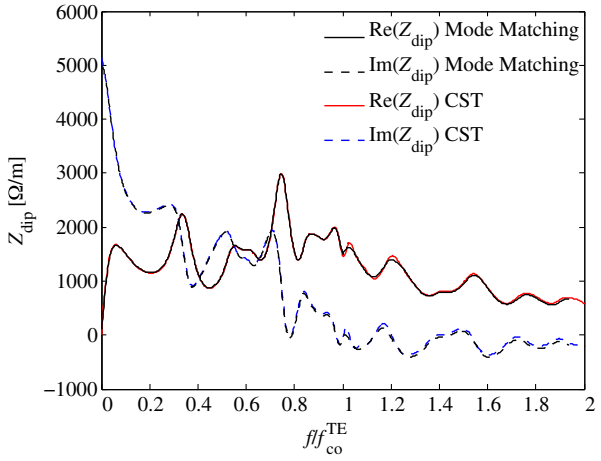

FIG. 8. Comparison of mode matching and CST. Mode matching parameters: $b = 5$ cm, $t = 25$ cm, $L = 20$ cm, $\sigma_c = 10^{-2}$ S/m, $\beta = 1$, $P = 15$, $S = 15$. CST parameters: $\sigma_b = 2$ cm, $L_{\mathrm{wake}} = 20$ m, $N_{\mathrm{mesh}} = 3.8 \times 10^6$.

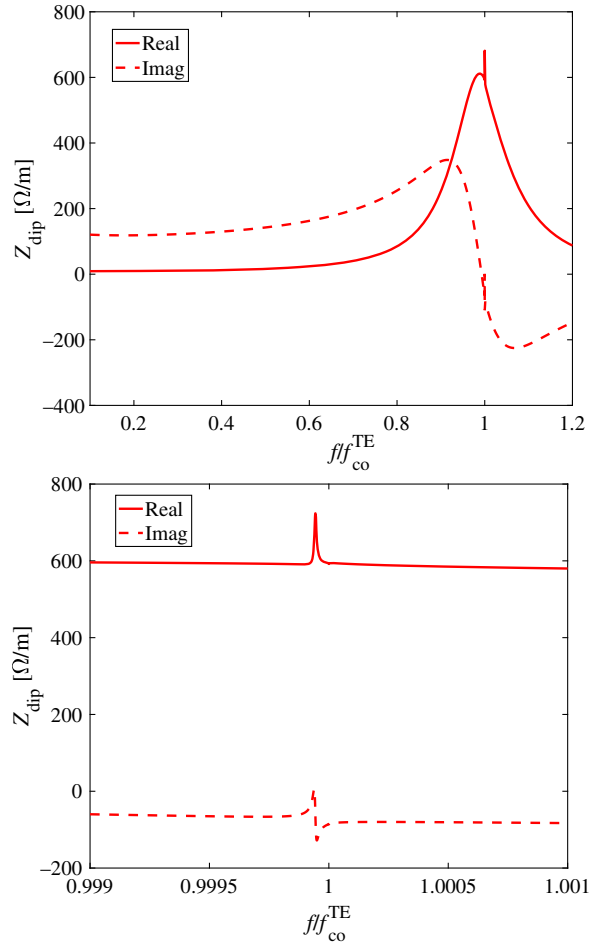

FIG. 9. Perturbation of the dipolar impedance by a trapped mode close to the TE_{11} cutoff frequency (top) and enlarged view around cutoff (bottom). Mode matching parameters: $b = 10$ cm, $t = 10$ cm, $L = 1/8\lambda^{\mathrm{TE}}_{co}$, $\sigma = 10^{-2}$ S/m, $\beta = 1$, $P = 5$, $S = 25$.

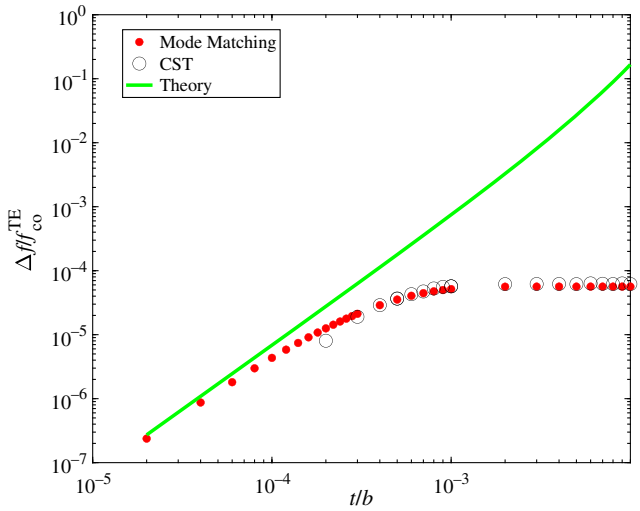

FIG. 10. Relative trapped mode frequency shift in the dipolar impedance with respect to TE_{11} cutoff frequency for different relative thicknesses t/b. Comparison among mode matching, CST simulations and theory of [24]. Mode matching parameters: $b = 10$ cm, $L = 1/8\lambda_{co}^{TE}$, $\sigma = 10^{-2}$ S/m, $\beta = 1$, $P = 5$, $S = 25$.

method and the mode matching for very small cavity thicknesses, a deviation from the perturbative theory starts to appear when $t/b > 10^{-4}$. CST simulations have been performed from $t/b \geq 2 \times 10^{-4}$ due to practical meshing limits. This study further confirms the mode matching flexibility and reliability as a tool to evaluate the dipolar impedance over a wide range of parameters.

F. Impedance dependence on relativistic β

We now benchmark the mode matching method for impedance calculation in the case of non-ultrarelativistic beam velocities, i.e., $\beta < 1$. This problem is of interest to machines working in the first stages of beam acceleration. For example, in the CERN Low Energy Ion Ring (LEIR), the Pb54+ beam is first injected at 4.2 MeV/nucleon and accelerated to 72.2 MeV/nucleon, which corresponds to a swing in relativistic β from 0.09 to 0.37. At low β, effects like space charge (SC) become relevant for the beam dynamics and play a key role in the overall beam stability.

The resistive wall impedance of circular vacuum chambers in the low β regime was already studied in the past in [25] and [26] and generalized within the IW2D code [21]. These approaches are all valid for infinitely long beam pipes, i.e., where edge effects and/or cavity resonances are not expected to appear.

Since the source fields for the impedance calculations are the fields produced by a beam traveling in a perfectly conducting beam pipe, the impedance calculated with the mode matching does not take into account the direct and indirect space charge (DSC and ISC). The DSC represents the direct interaction of the source particle field with the test particle, the ISC the interaction with the scattered fields of the perfectly conducting beam pipe. Since in the IW2D code, the ISC impedance is embedded in the impedance calculation, we add the Z^{ISC} term to the impedance calculated with the mode matching.

The ISC transverse impedance per unit meter in a round beam pipe of radius b is given by [15]

$$Z_{dip}^{ISC} = \frac{jI_1^2(s)Z_o}{\beta\gamma^2\pi r_S^2}\frac{K_1(x)}{I_1(x)}. \tag{61}$$

For $r_S \to 0$, the expressions simplify to

$$Z_{dip}^{ISC} = \frac{j\omega^2 Z_o}{4\pi c^2\beta^3\gamma^4}\frac{K_1(x)}{I_1(x)}. \tag{62}$$

For small argument of x, we recover the well-known formulas showing the $1/\gamma^2$ dependence

$$Z_{dip}^{ISC} = \frac{jZ_o}{2\pi\beta\gamma^2}\frac{1}{b^2}. \tag{63}$$

Figure 11 shows the comparison between IW2D code and the mode matching for a high conductivity material. The reader can appreciate the very good agreement between the two codes for varying β. Also, as described in detail in [12], both real and imaginary parts exhibit a roll-off behavior at high frequencies due to the finite beam spectrum for $\beta \neq 1$.

The ultrarelativistic beam approximation, commonly used in impedance calculations, constitutes, in the case of the real part of the impedance, the worst-case scenario. The discrepancy at low frequencies is due to the PEC

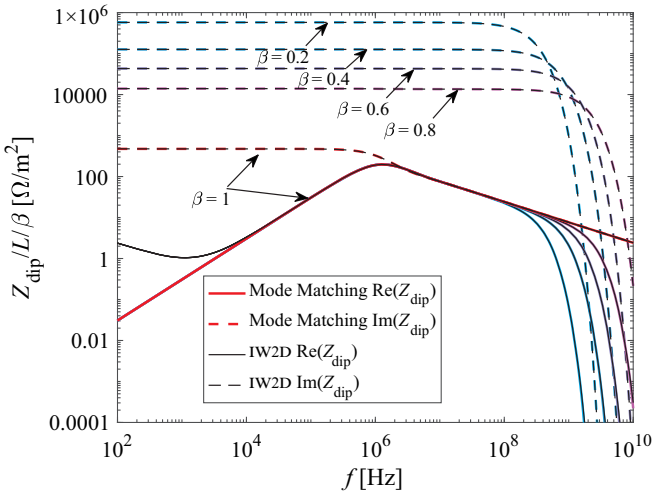

FIG. 11. Comparison between the mode matching and IW2D code for different relativistic β. The thick line is the real part and the dashed line is the imaginary part of the impedance. The transverse impedance is normalized over β. Mode matching parameters: $b = 0.05$ m, $t = 0.5$ mm, $L = 20$ cm, $\sigma = 10^6$ S/m, $\beta = (0.2, 0.4, 0.6, 0.8, 1)$, $P = 25$, $S = 25$.

approximation made in the IW2D code, for which we considered a layer with high conductivity ($\sigma = 10^{14}$ S/m).

V. CONCLUSION

In this work, we presented the application of the mode matching method for the calculation of the transverse driving impedance of a cylindrical cavity loaded with a toroidal insert. While the same method has been applied in the past for the computation of longitudinal impedances, it is the first time that it is implemented for the transverse case. Notably, the inclusion of the full set of solenoidal and irrotational modes is necessary to correctly compute the impedance.

Despite the simplicity of the chosen geometry, the model can serve as a first impedance estimator for various devices (e.g., lossy inserts, flanges, resistive beam pipes, collimators, ferrite loaded cavities, etc.) allowing flexible and accurate parametric explorations (see, e.g., the application performed in [27]). An extensive set of benchmark results against available analytical formulas, field matching codes, and commercial solvers has been performed highlighting the method's reliability and good performance over a wide range of parameters.

After having demonstrated the rapid convergence of the method, we successfully benchmarked the approach for an empty cavity, a cavity at low frequency and a resistive wall impedance in both low and intermediate frequency regimes. For this last case, we investigated the validity of the 2D infinite length approximation for the computation of resistive wall impedance showing that this is valid only for devices whose length is larger than the transverse direction. We also successfully compared the method against CST time domain simulations for structures where analytical formulas are not available. Moreover, the presence of trapped modes introduced by small beam pipe deformations has been investigated and compared to perturbative methods and CST time domain simulations. Since the used approach is non-ultrarelativistic, we also performed a benchmark of the impedance behavior as a function of the relativistic particle beam velocity.

Based on these results, the method proved to be a powerful new tool for the evaluation of the impedance of accelerator devices. The generalization of the method to arbitrary cavity geometries is currently being addressed by performing a 3D numerical modal decomposition (e.g., with the Eigenmode solver of CST) in place of the analytical one performed for the geometry addressed in this work. This would allow a direct computation of the impedance in frequency domain for structures more general than the ones treated in this work.

ACKNOWLEDGMENTS

The authors thank the late Professor Vittorio Giorgio Vaccaro for all his indispensable work in the conception of this methodology, for his infinite curiosity and humanity.

APPENDIX A: FIELD TABLES

The fields are defined with the following parameters:
(i) α_p: pth zero of the Bessel function $J_\nu(x)$ with $\nu = 1$.
(ii) β_p: pth zero of the Bessel function $J'_\nu(x)$ with $\nu = 1$.
(iii) J'_1: derivative of Bessel J_1 function with respect to r.
(iv) k_o: characteristic constant in vacuum $k_o = \omega\sqrt{\mu_o\varepsilon_o}$.
(v) k_f: characteristic constant in the insert material $k_f = \omega\sqrt{\mu_f\varepsilon_f}$.
(vi) Z_o: characteristic impedance in vacuum $Z_o = \sqrt{\mu_o/\varepsilon_o}$.
(vii) Z_f: characteristic impedance in the insert material $Z_f = \sqrt{\mu_f/\varepsilon_f}$.
(viii) α_o: normalized characteristic constant in vacuum $\alpha_o = k_o b$.
(ix) α_f: normalized characteristic constant in the insert material $\alpha_f = k_f b$.

TABLE II. TM scattered field components (subdomains I–III).

Scattered fields TM	Left pipe (I)	Right pipe (II)	Insert (III)
E_r	$\frac{j\,b\,J'_1(\frac{r\alpha_p}{b})\cos(\phi)\tilde{\alpha}_p}{\alpha_p^2\mathcal{T}_s^{\mathrm{TM}}}e^{\frac{jz\tilde{\alpha}_p}{b}}$	$-\frac{j\,b\,J'_1(\frac{r\alpha_p}{b})\cos(\phi)\tilde{\alpha}_p}{\alpha_p^2\mathcal{T}_s^{\mathrm{TM}}}e^{-\frac{j(z-L)\tilde{\alpha}_p}{b}}$	$-\frac{\alpha_s\,\cos(\phi)\sin(\frac{z\alpha_s}{b})\mathcal{W}'_{\mathrm{TMs}}(\frac{r\tilde{\alpha}_{fs}}{b})}{\mathcal{L}_s^{\mathrm{TM}}\tilde{\alpha}_{fs}}$
E_ϕ	$-\frac{j\,b\,\sin(\phi)\tilde{\alpha}_p J_1(\frac{r\alpha_p}{b})}{r\alpha_p^2\mathcal{T}_s^{\mathrm{TM}}}e^{\frac{jz\tilde{\alpha}_p}{b}}$	$\frac{j\,b\,\sin(\phi)\tilde{\alpha}_p J_1(\frac{r\alpha_p}{b})}{r\alpha_p^2\mathcal{T}_s^{\mathrm{TM}}}e^{-\frac{j(z-L)\tilde{\alpha}_p}{b}}$	$\frac{b\,\alpha_s\,\sin(\phi)\sin(\frac{z\alpha_s}{b})\mathcal{W}_{\mathrm{TMs}}(\frac{r\tilde{\alpha}_{fs}}{b})}{r\mathcal{L}_s^{\mathrm{TM}}\tilde{\alpha}_{fs}^2}$
E_z	$\frac{\cos(\phi)J_1(\frac{r\alpha_p}{b})}{\mathcal{T}_s^{\mathrm{TM}}}e^{\frac{jz\tilde{\alpha}_p}{b}}$	$\frac{\cos(\phi)J_1(\frac{r\alpha_p}{b})}{\mathcal{T}_s^{\mathrm{TM}}}e^{-\frac{j(z-L)\tilde{\alpha}_p}{b}}$	$\frac{\cos(\phi)\cos(\frac{z\alpha_s}{b})\mathcal{W}_{\mathrm{TMs}}(\frac{r\tilde{\alpha}_{fs}}{b})}{\mathcal{L}_s^{\mathrm{TM}}}$
H_r	$-\frac{j\,b\,\alpha_o\,\sin(\phi)J_1(\frac{r\alpha_p}{b})}{rZ_o\alpha_p^2\mathcal{T}_s^{\mathrm{TM}}}e^{\frac{jz\tilde{\alpha}_p}{b}}$	$-\frac{j\,b\,\alpha_o\,\sin(\phi)J_1(\frac{r\alpha_p}{b})}{rZ_o\alpha_p^2\mathcal{T}_s^{\mathrm{TM}}}e^{-\frac{j(z-L)\tilde{\alpha}_p}{b}}$	$-\frac{j\,b\,\alpha_f\,\sin(\phi)\cos(\frac{z\alpha_s}{b})\mathcal{W}_{\mathrm{TMs}}(\frac{r\tilde{\alpha}_{fs}}{b})}{rZ_f\mathcal{L}_s^{\mathrm{TM}}\tilde{\alpha}_{fs}^2}$
H_ϕ	$\frac{-j\,b\,\alpha_o\cos(\phi)J'_1(\frac{r\alpha_p}{b})}{Z_o\alpha_p^2\mathcal{T}_s^{\mathrm{TM}}}e^{\frac{jz\tilde{\alpha}_p}{b}}$	$\frac{-j\,b\,\alpha_o\cos(\phi)J'_1(\frac{r\alpha_p}{b})}{Z_o\alpha_p^2\mathcal{T}_s^{\mathrm{TM}}}e^{-\frac{j(z-L)\tilde{\alpha}_p}{b}}$	$-\frac{j\,\alpha_f\,\cos(\phi)\cos(\frac{z\alpha_s}{b})\mathcal{W}'_{\mathrm{TMs}}(\frac{r\tilde{\alpha}_{fs}}{b})}{Z_f\mathcal{L}_s^{\mathrm{TM}}\tilde{\alpha}_{fs}}$
H_z	0	0	0

TABLE III. TE scattered field components (subdomains I–III).

Scattered fields TE	Left pipe (I)	Right pipe (II)	Insert (III)
E_r	$-\frac{j\,b\,\alpha_o\,\cos(\phi)J_1(\frac{r\beta_p}{b})}{rY_0\beta_p^2\mathcal{T}_p^{\mathrm{TE}}}e^{\frac{jz\tilde{\beta}_p}{b}}$	$-\frac{j\,b\,\alpha_o\,\cos(\phi)J_1(\frac{r\beta_p}{b})}{rY_0\beta_p^2\mathcal{T}_p^{\mathrm{TE}}}e^{-\frac{j(z-L)\tilde{\beta}_p}{b}}$	$-\frac{j\,b\,\alpha_f\,\cos(\phi)\sin(\frac{z\alpha_s}{b})\mathcal{W}_{\mathrm{TEs}}(\frac{r\tilde{\alpha}_{fs}}{b})}{\mathcal{L}_s^{\mathrm{TE}}rY_f\tilde{\alpha}_{fs}^2}$
E_ϕ	$\frac{j\,b\,\alpha_o\,\sin(\phi)J_1'(\frac{r\beta_p}{b})}{Y_0\beta_p^2\mathcal{T}_p^{\mathrm{TE}}}e^{\frac{jz\tilde{\beta}_p}{b}}$	$-\frac{j\,b\,\alpha_o\,\sin(\phi)J_1'(\frac{r\beta_p}{b})}{Y_0\beta_p^2\mathcal{T}_p^{\mathrm{TE}}}e^{-\frac{j(z-L)\tilde{\beta}_p}{b}}$	$\frac{j\,\alpha_f\,\sin(\phi)\sin(\frac{z\alpha_s}{b})\mathcal{W}'_{\mathrm{TEs}}(\frac{r\tilde{\alpha}_{fs}}{b})}{\mathcal{L}_s^{\mathrm{TE}}Y_f\tilde{\alpha}_{fs}}$
E_z	0	0	0
H_r	$\frac{j\,b\,J_1'(\frac{r\beta_p}{b})\sin(\phi)\tilde{\beta}_p}{\sqrt{2\pi}\beta_p^2\mathcal{T}_p^{\mathrm{TE}}}e^{\frac{jz\tilde{\beta}_p}{b}}$	$-\frac{j\,b\,J_1'(\frac{r\beta_p}{b})\sin(\phi)\tilde{\beta}_p}{\beta_p^2\mathcal{T}_p^{\mathrm{TE}}}e^{-\frac{j(z-L)\tilde{\beta}_p}{b}}$	$\frac{\alpha_s\,\sin(\phi)\cos(\frac{z\alpha_s}{b})\mathcal{W}'_{\mathrm{TEs}}(\frac{r\tilde{\alpha}_{fs}}{b})}{\mathcal{L}_s^{\mathrm{TE}}\tilde{\alpha}_{fs}}$
H_ϕ	$\frac{j\,b\,\cos(\phi)\tilde{\beta}_pJ_1(\frac{r\beta_p}{b})}{r\beta_p^2\mathcal{T}_p^{\mathrm{TE}}}e^{\frac{jz\tilde{\beta}_p}{b}}$	$-\frac{j\,b\,\cos(\phi)\tilde{\beta}_pJ_1(\frac{r\beta_p}{b})}{r\beta_p^2\mathcal{T}_p^{\mathrm{TE}}}e^{-\frac{j(z-L)\tilde{\beta}_p}{b}}$	$\frac{b\,\alpha_s\,\cos(\phi)\cos(\frac{z\alpha_s}{b})\mathcal{W}_{\mathrm{TEs}}(\frac{r\tilde{\alpha}_{fs}}{b})}{\mathcal{L}_s^{\mathrm{TE}}r\tilde{\alpha}_{fs}^2}$
H_z	$\frac{\sin(\phi)J_1(\frac{r\beta_p}{b})}{\mathcal{T}_p^{\mathrm{TE}}}e^{\frac{jz\tilde{\beta}_p}{b}}$	$\frac{\sin(\phi)J_1(\frac{r\beta_p}{b})}{\mathcal{T}_p^{\mathrm{TE}}}e^{-\frac{j(z-L)\tilde{\beta}_p}{b}}$	$\frac{\sin(\phi)\sin(\frac{z\alpha_s}{b})\mathcal{W}_{\mathrm{TEs}}(\frac{r\tilde{\alpha}_{fs}}{b})}{\mathcal{L}_s^{\mathrm{TE}}}$

(x) $\tilde{\alpha}_p$: beam pipe normalized propagation constant $\tilde{\alpha}_p=\sqrt{\alpha_o^2-\alpha_p^2}$.

(xi) α_s: longitudinal normalized cavity TM eigenvalue $\alpha_s=s\pi\frac{b}{L}$.

(xii) β_s: longitudinal normalized cavity TE eigenvalue $\beta_s=\alpha_s$.

(xiii) $\tilde{\alpha}_{fs}$: radial normalized propagation constant in the insert $\tilde{\alpha}_{fs}=\sqrt{\alpha_f^2-\alpha_s^2}$.

(xiv) $\alpha_{p\,s}$: cavity TM eigenvalues $\alpha_{p\,s}=\sqrt{\alpha_p^2+\alpha_s^2}$.

(xv) $\beta_{p\,s}$: cavity TE eigenvalues $\beta_{p\,s}=\sqrt{\beta_p^2+\beta_s^2}$.

(xvi) $\mathcal{W}_{\mathrm{TMs}}$: radial TM wave function in the insert $\mathcal{W}_{\mathrm{TMs}}(r)=H_\nu^{(2)}(\frac{r\tilde{\alpha}_{fs}}{b})-\frac{H_\nu^{(2)}(\frac{c\tilde{\alpha}_{fs}}{b})}{H_\nu^{(1)}(\frac{c\tilde{\alpha}_{fs}}{b})}H_\nu^{(1)}(\frac{r\tilde{\alpha}_{fs}}{b})$ calculated in $r=b$ with $\nu=1$.

(xvii) $\mathcal{W}'_{\mathrm{TMs}}$: derivative of $\mathcal{W}_{\mathrm{TMs}}(r)$ with respect to r calculated in $r=b$.

(xviii) $\mathcal{W}_{\mathrm{TEs}}$: radial TE wave function in the insert $\mathcal{W}_{\mathrm{TEs}}(r)=H_\nu^{(2)}(\frac{r\tilde{\alpha}_{fs}}{b})-\frac{H_\nu'^{(2)}(\frac{c\tilde{\alpha}_{fs}}{b})}{H_\nu'^{(1)}(\frac{c\tilde{\alpha}_{fs}}{b})}H_\nu^{(1)}(\frac{r\tilde{\alpha}_{fs}}{b})$ calculated in $r=b$ with $\nu=1$.

(xix) $\mathcal{W}'_{\mathrm{TEs}}$: derivative of $\mathcal{W}_{\mathrm{TEs}}(r)$ with respect to r calculated in $r=b$.

(xx) $\mathcal{V}_{p\,s}^{\mathrm{TM}}$: norm of solenoidal modes $\mathcal{V}_{p\,s}^{\mathrm{TM}}=b\sqrt{\frac{\pi}{2}}\sqrt{\frac{L}{\epsilon_s}}J_0(\alpha_p)\frac{\alpha_{p\,s}}{\alpha_p}$.

(xxi) $\mathcal{V}_{p\,s}^{\mathrm{TE}}$: norm of solenoidal modes $\mathcal{V}_{p\,s}^{\mathrm{TE}}=b\sqrt{\frac{\pi}{2}}\sqrt{\frac{L}{2}}\sqrt{\beta_p^2-1}J_0(\beta_p)\frac{\beta_{p\,s}}{\beta_p}$.

(xxii) $\mathcal{V}_{p\,s}^{\mathrm{E}}$: norm of electric irrotational modes $\mathcal{V}_{p\,s}^{\mathrm{E}}=\frac{1}{2}\sqrt{\pi}\sqrt{L}\alpha_{p\,s}J_0(\alpha_p)$.

(xxiii) $\mathcal{V}_{p\,s}^{\mathrm{H}}$: norm of magnetic irrotational modes $\mathcal{V}_{p\,s}^{\mathrm{H}}=\sqrt{\frac{\pi}{2}}\beta_{p\,s}J_0(\beta_p)\sqrt{\frac{L}{\epsilon_s}}\sqrt{\beta_p^2-1}$.

(xxiv) $\mathcal{T}_p^{\mathrm{TE}}$: transverse norm $\mathcal{T}_p^{\mathrm{TE}}=\sqrt{\frac{\pi}{2}}\beta_p\sqrt{\beta_p^2-1}J_0(\beta_p)$.

(xxv) $\mathcal{T}_p^{\mathrm{TM}}$: transverse norm $\mathcal{T}_p^{\mathrm{TM}}=\sqrt{\frac{\pi}{2}}\alpha_pJ_0(\alpha_p)$.

TABLE IV. Scattered field components (subdomain IV).

Scattered fields	Solenoidal TM	Solenoidal TE	Irrotational
E_r	$-\frac{b\,\alpha_s\,\cos(\phi)J_1'(\frac{r\alpha_p}{b})\sin(\frac{z\alpha_s}{b})}{\alpha_p^2\mathcal{V}_p^{\mathrm{TM}}}$	$\frac{b\,\beta_{p\,s}\,\cos(\phi)J_1(\frac{r\beta_p}{b})\sin(\frac{z\alpha_s}{b})}{r\beta_p^2\mathcal{V}_p^{\mathrm{TE}}}$	$\frac{\cos(\phi)J_1'(\frac{r\alpha_p}{b})\sin(\frac{z\alpha_s}{b})}{\mathcal{V}_p^E}$
E_ϕ	$\frac{b\,\alpha_s\,\sin(\phi)J_1(\frac{r\alpha_p}{b})\sin(\frac{z\alpha_s}{b})}{r\alpha_p^2\mathcal{V}_p^{\mathrm{TM}}}$	$-\frac{b\,\beta_{p\,s}\,\sin(\phi)J_1'(\frac{r\beta_p}{b})\sin(\frac{z\alpha_s}{b})}{\beta_p^2\mathcal{V}_p^{\mathrm{TE}}}$	$-\frac{\sin(\phi)J_1(\frac{r\alpha_p}{b})\sin(\frac{z\alpha_s}{b})}{r\mathcal{V}_p^E}$
E_z	$\frac{\cos(\phi)J_1(\frac{r\alpha_p}{b})\cos(\frac{z\alpha_s}{b})}{\mathcal{V}_p^{\mathrm{TM}}}$	0	$\frac{\alpha_s\,\cos(\phi)J_1(\frac{r\alpha_p}{b})\cos(\frac{z\alpha_s}{b})}{b\mathcal{V}_p^E}$
H_r	$-\frac{b\,\alpha_{p\,s}\,\sin(\phi)J_1(\frac{r\alpha_p}{b})\cos(\frac{z\alpha_s}{b})}{r\alpha_p^2\mathcal{V}_p^{\mathrm{TM}}}$	$\frac{b\,\alpha_s\,\sin(\phi)J_1'(\frac{r\beta_p}{b})\cos(\frac{z\alpha_s}{b})}{\beta_p^2\mathcal{V}_p^{\mathrm{TE}}}$	$\frac{\sin(\phi)J_1'(\frac{r\beta_p}{b})\cos(\frac{z\alpha_s}{b})}{\mathcal{V}_p^H}$
H_ϕ	$-\frac{b\,\alpha_{p\,s}\,\cos(\phi)J_1'(\frac{r\alpha_p}{b})\cos(\frac{z\alpha_s}{b})}{\alpha_p^2\mathcal{V}_p^{\mathrm{TM}}}$	$\frac{b\,\alpha_s\,\cos(\phi)J_1(\frac{r\beta_p}{b})\cos(\frac{z\alpha_s}{b})}{r\beta_p^2\mathcal{V}_p^{\mathrm{TE}}}$	$\frac{\cos(\phi)J_1(\frac{r\beta_p}{b})\cos(\frac{z\alpha_s}{b})}{r\mathcal{V}_p^H}$
H_z	0	$\frac{\sin(\phi)J_1(\frac{r\beta_p}{b})\sin(\frac{z\alpha_s}{b})}{\mathcal{V}_p^{\mathrm{TE}}}$	$-\frac{\alpha_s\,\sin(\phi)J_1(\frac{r\beta_p}{b})\sin(\frac{z\alpha_s}{b})}{b\mathcal{V}_p^H}$

(xxvi) $\mathcal{L}_s^{\mathrm{TM}}$: longitudinal TM norm $\mathcal{L}_s^{\mathrm{TM}} = \sqrt{L/\epsilon_s}$.

(xxvii) $\mathcal{L}_s^{\mathrm{TE}}$: longitudinal TE norm $\mathcal{L}_s^{\mathrm{TE}} = \sqrt{L/2}$.

In order to correctly represent the reflected waves in the beam pipes, we chose α_p with $\mathrm{Re}(\alpha_p) > 0$ and $\mathrm{Im}(\alpha_p) < 0$: in this way, the scattered waves below cutoff get attenuated in both subdomains I and II. Analogous considerations hold for β_p.

APPENDIX B: SERIES SUMMATIONS

Here we list the sums of series used to simplify the mode matching. Sum of series in s:

$$\sum_{s=0}^{\infty} \frac{\epsilon_s}{\alpha_0^2 - \alpha_{p\,s}^2} = \frac{L}{b\tilde{\alpha}_p} \cot\left(\frac{L\tilde{\alpha}_p}{b}\right), \tag{B1}$$

$$\sum_{s=0}^{\infty} \frac{(-1)^s \epsilon_s}{\alpha_0^2 - \alpha_{p\,s}^2} = \frac{L}{b\tilde{\alpha}_p} \csc\left(\frac{L\tilde{\alpha}_p}{b}\right), \tag{B2}$$

$$\sum_{s=0}^{\infty} \frac{\epsilon_s}{\beta_{p\,s}^2} = \frac{L}{b\beta_p} \coth\left(\frac{L\beta_p}{b}\right), \tag{B3}$$

$$\sum_{s=0}^{\infty} \frac{(-1)^s \epsilon_s}{\beta_{p\,s}^2} = \frac{L}{b\beta_p} \mathrm{csch}\left(\frac{L\beta_p}{b}\right), \tag{B4}$$

$$\sum_{s=0}^{\infty} \frac{\alpha_s^2}{\beta_{p\,s}^2(\alpha_0^2 - \beta_{p\,s}^2)} = \frac{L}{2b\alpha_0^2} \left[\tilde{\beta}_p \cot\left(\frac{L\tilde{\beta}_p}{b}\right) - \beta_p \coth\left(\frac{L\beta_p}{b}\right)\right], \tag{B5}$$

$$\sum_{s=0}^{\infty} \frac{(-1)^s \alpha_s^2}{\beta_{p\,s}^2(\alpha_0^2 - \beta_{p\,s}^2)} = \frac{L}{2b\alpha_0^2} \left[\tilde{\beta}_p \csc\left(\frac{L\tilde{\beta}_p}{b}\right) - \beta_p \mathrm{csch}\left(\frac{L\beta_p}{b}\right)\right], \tag{B6}$$

$$\sum_{s=0}^{\infty} \frac{(-1)^s \epsilon_s (\alpha_o^2 - \alpha_s^2)(-1 + (-1)^s e^{\frac{jL\alpha_b}{b}})}{(\alpha_b^2 - \alpha_s^2)(\alpha_o^2 - \alpha_{p\,s}^2)} = \frac{L\{i\tilde{\alpha}_p e^{\frac{jL\alpha_b}{b}}(\alpha_b^2 - \alpha_o^2) + \alpha_b \alpha_p^2[-\csc(\frac{L\tilde{\alpha}_p}{b}) + e^{\frac{jL\alpha_b}{b}} \cot(\frac{L\tilde{\alpha}_p}{b})]\}}{b\alpha_b \tilde{\alpha}_p (\alpha_b^2 - \alpha_o^2 + \alpha_p^2)}, \tag{B7}$$

$$\sum_{s=0}^{\infty} \frac{\epsilon_s (\alpha_o^2 - \alpha_s^2)(-1 + (-1)^s e^{\frac{jL\alpha_b}{b}})}{(\alpha_b^2 - \alpha_s^2)(\alpha_o^2 - \alpha_{p\,s}^2)} = \frac{L\{\alpha_b \alpha_p^2[-\cot(\frac{L\tilde{\alpha}_p}{b}) + e^{\frac{jL\alpha_b}{b}} \csc(\frac{L\tilde{\alpha}_p}{b})] + i\tilde{\alpha}_p(\alpha_b^2 - \alpha_o^2)\}}{b\alpha_b \tilde{\alpha}_p (\alpha_b^2 - \alpha_o^2 + \alpha_p^2)}, \tag{B8}$$

$$\sum_{s=0}^{\infty} \frac{\alpha_s^2 (-1 + (-1)^s e^{\frac{jL\alpha_b}{b}})}{(\alpha_b^2 - \alpha_s^2)(\beta_p^2 + \beta_s^2)} = \frac{L[i\alpha_b + \beta_p \mathrm{csch}(\frac{L\beta_p}{b})(\cosh(\frac{L\beta_p}{b}) - e^{\frac{jL\alpha_b}{b}})]}{2b(\alpha_b^2 + \beta_p^2)}, \tag{B9}$$

$$\sum_{s=0}^{\infty} \frac{(-1)^s \alpha_s^2 (-1 + (-1)^s e^{\frac{jL\alpha_b}{b}})}{(\alpha_b^2 - \alpha_s^2)(\beta_p^2 + \beta_s^2)} = \frac{L\beta_p \mathrm{csch}(\frac{L\beta_p}{b}) + iLe^{\frac{jL\alpha_b}{b}}[\alpha_b + i\beta_p \coth(\frac{L\beta_p}{b})]}{2b(\alpha_b^2 + \beta_p^2)}, \tag{B10}$$

$$\sum_{s=0}^{\infty} \frac{\epsilon_s (-1 + (-1)^s e^{\frac{jL\alpha_b}{b}})}{(\alpha_b^2 - \alpha_s^2)(\beta_p^2 + \beta_s^2)} = \frac{-L\alpha_b \coth(\frac{L\beta_p}{b}) + L\alpha_b e^{\frac{jL\alpha_b}{b}} \mathrm{csch}(\frac{L\beta_p}{b}) + iL\beta_p}{b\alpha_b^3 \beta_p + b\alpha_b \beta_p^3}, \tag{B11}$$

$$\sum_{s=0}^{\infty} \frac{\epsilon_s (e^{\frac{jL\alpha_b}{b}} - (-1)^s)}{(\alpha_b^2 - \alpha_s^2)(\beta_p^2 + \beta_s^2)} = \frac{jL\beta_p e^{\frac{jL\alpha_b}{b}} + L\alpha_b e^{\frac{jL\alpha_b}{b}} \coth(\frac{L\beta_p}{b}) - L\alpha_b \,\mathrm{csch}(\frac{L\beta_p}{b})}{b\alpha_b^3 \beta_p + b\alpha_b \beta_p^3}. \tag{B12}$$

Sum of series in p.

$$\sum_{p=1}^{\infty} \frac{1}{\alpha_0^2 - \alpha_{p\,s}^2} = -\frac{1}{2\tilde{\alpha}_s} \frac{J_2(\tilde{\alpha}_s)}{J_1(\tilde{\alpha}_s)}, \tag{B13}$$

$$\sum_{p=1}^{\infty} \frac{\beta_p^2}{(\beta_p^2 - 1)\beta_{p\,s}^2(\alpha_0^2 - \beta_{p\,s}^2)} = \frac{1}{\alpha_0^2} \left(\frac{J_0(\alpha_s) - I_2(\alpha_s)}{2[I_0(\alpha_s) + I_2(\alpha_s)]} - \frac{J_0(\tilde{\alpha}_s) + J_2(\tilde{\alpha}_s)}{2[J_0(\tilde{\alpha}_s) - J_2(\tilde{\alpha}_s)]}\right), \tag{B14}$$

$$\sum_{p=1}^{\infty} \frac{1}{(\beta_p^2 - 1)\beta_{p\,s}^2(\alpha_0^2 - \beta_{p\,s}^2)} = \frac{1}{\alpha_0^2} \left(\frac{J_2(\tilde{\alpha}_s)/\tilde{\alpha}_s}{2[J_1(\tilde{\alpha}_s) - \tilde{\alpha}_s J_0(\tilde{\alpha}_s)]} + \frac{J_2(\alpha_s)/\alpha_s}{2[\alpha_s I_0(\alpha_s) - I_1(\alpha_s)]}\right), \tag{B15}$$

$$\sum_{p=1}^{\infty}\frac{1}{(\beta_p^2-1)(\alpha_0^2-\beta_{p\,s}^2)}=\frac{1}{2\tilde{\alpha}_s}\frac{J_2(\tilde{\alpha}_s)}{J_1(\tilde{\alpha}_s)-\tilde{\alpha}_s J_0(\tilde{\alpha}_s)}, \tag{B16}$$

$$\sum_{p=1}^{\infty}\frac{\beta_p^2}{(\beta_p^2-1)\beta_{p\,s}^2}=\frac{1}{2}\frac{J_0(\alpha_s)-I_2(\alpha_s)}{I_0(\alpha_s)+I_2(\alpha_s)}, \tag{B17}$$

$$\sum_{p=1}^{\infty}\frac{\beta_p^2}{(\beta_p^2-1)(\alpha_0^2-\beta_{p\,s}^2)}=-\frac{1}{2}\frac{J_0(\tilde{\alpha}_s)+J_2(\tilde{\alpha}_s)}{J_0(\tilde{\alpha}_s)-J_2(\tilde{\alpha}_s)}, \tag{B18}$$

$$\sum_{p=1}^{\infty}\frac{\beta_p^4}{(\beta_p^2-1)\beta_{p\,s}^2(\alpha_0^2-\beta_{p\,s}^2)}=-\frac{1}{2\alpha_0^2}\left(\frac{\tilde{\alpha}_s^2[J_0(\tilde{\alpha}_s)+J_2(\tilde{\alpha}_s)]}{J_0(\tilde{\alpha}_s)-J_2(\tilde{\alpha}_s)}+\frac{\beta_s^2[I_0(\alpha_s)-I_2(\alpha_s)]}{J_0(\alpha_s)+I_2(\alpha_s)}\right), \tag{B19}$$

$$\sum_{p=1}^{\infty}\frac{1}{J_2(\alpha_p)(\alpha_o^2-\alpha_{p\,s}^2)}=\frac{1}{\tilde{\alpha}_s^2}-\frac{1}{2\tilde{\alpha}_s J_1(\tilde{\alpha}_s)}, \tag{B20}$$

$$\sum_{p=1}^{\infty}\frac{\beta_p^2}{(\beta_p^2-1)J_0(\beta_p)\beta_{p\,s}^2}=-\frac{\beta_s^2}{2\beta_s I_1(\beta_s)-2\beta_s^2 I_0(\beta_s)}, \tag{B21}$$

$$\sum_{p=1}^{\infty}\frac{\beta_{p\,s}^2-\alpha_f^2}{(\beta_p^2-1)J_0(\beta_p)\beta_{p\,s}^2}=1-\alpha_f^2\left(\frac{1}{\beta_s^2}+\frac{1}{2\beta_s I_1(\beta_s)-2\beta_s^2 I_0(\beta_s)}\right). \tag{B22}$$

APPENDIX C: MATRIX ELEMENTS

$$\mathrm{N1}_{pp}=\sqrt{\frac{\pi}{2}}\frac{\alpha_p^2}{L}, \tag{C1}$$

$$\mathrm{M1}_{p\,s}=\frac{\sqrt{L\epsilon_s}(1-(-1)^s e^{-\frac{jL\tilde{\alpha}_p}{b}})\mathcal{W}_{\mathrm{TMs}}(\tilde{\alpha}_{fs})}{\alpha_o^2-\alpha_{p\,s}^2}, \tag{C2}$$

$$\mathrm{II}_{ss}=(-1)^s, \tag{C3}$$

$$\mathrm{N2}_{pp}=-\frac{j\sqrt{\pi}\beta_p^2}{4\sqrt{L}Y_f\alpha_o Z_o\sqrt{\beta_p^2-1}\tilde{\beta}_p(\cot(\frac{L\tilde{\beta}_p}{b})+j)}, \tag{C4}$$

$$\mathrm{M2}_{p\,s}=\frac{2\alpha_f\beta_p^2\alpha_s\epsilon_s(\beta_{p\,s}^2-\alpha_o^2\delta_s)\mathcal{W}'_{\mathrm{TEs}}(\tilde{\alpha}_{fs})(\cot(\frac{L\tilde{\beta}_p}{b})-(-1)^s\csc(\frac{L\tilde{\beta}_p}{b})+j)}{\beta_{p\,s}^2\tilde{\alpha}_{fs}(\beta_{p\,s}^2-\alpha_o^2)}, \tag{C5}$$

$$\mathrm{M3}_{p\,s}=\frac{2j\sqrt{2\epsilon_s}Y_f(\alpha_o^2\alpha_s^2-\alpha_f^2\tilde{\beta}_p^2)\mathcal{W}_{\mathrm{TMs}}(\tilde{\alpha}_{fs})(\cot(\frac{L\tilde{\beta}_p}{b})-(-1)^s\csc(\frac{L\tilde{\beta}_p}{b})+j)}{\tilde{\alpha}_{fs}^2(\alpha_o^2-\beta_{p\,s}^2)}. \tag{C6}$$

$$\mathrm{B}_{s\,1}=-\frac{jQI_1(s)\alpha_b^2(1-(-1)^s e^{-\frac{jL\alpha_b}{b}})}{\pi b\gamma(\alpha_b^2-\alpha_s^2)I_1(\frac{\alpha_b}{\gamma})}, \tag{C7}$$

$$\mathrm{T1}_{s\,s}=b\sqrt{\frac{2}{\pi}}, \tag{C8}$$

$$\mathrm{T2}_{s\,s} = \sqrt{\frac{2}{\pi}}\alpha_o^2\alpha_s^2, \tag{C9}$$

$$\mathrm{T3}_{s\,s} = \sqrt{\frac{2}{\pi}}\frac{\alpha_o}{Z_o}, \tag{C10}$$

$$\mathrm{G1}_{s\,p} = \frac{1}{\sqrt{\beta_p^2 - 1}\beta_{p\,s}^2}, \tag{C11}$$

$$\mathrm{G2}_{s\,p} = \frac{1}{\beta_p^2\sqrt{\beta_p^2 - 1}\beta_{p\,s}^2(\alpha_o^2 - \beta_{p\,s}^2)}, \tag{C12}$$

$$\mathrm{G3}_{s\,p} = \frac{\tilde{\alpha}_p}{\alpha_p^2(\alpha_o^2 - \alpha_{p\,s}^2)}, \tag{C13}$$

$$\mathrm{F1}_{s\,s} = \frac{\sqrt{L}\alpha_f\alpha_s[I_0(\alpha_s) - I_2(\alpha_s)]\mathcal{W}'_{\mathrm{TEs}}(\tilde{\alpha}_{fs})}{\sqrt{2}Y_f\alpha_o Z_o[I_0(\alpha_s) + I_2(\alpha_s)]\tilde{\alpha}_{fs}} - \frac{\sqrt{L}\alpha_s\mathcal{W}_{\mathrm{TEs}}(\tilde{\alpha}_{fs})}{\sqrt{2}\tilde{\alpha}_{fs}^2}, \tag{C14}$$

$$\begin{aligned}\mathrm{F2}_{ss} = -\frac{j\sqrt{L}}{2}\Bigg[&\frac{1}{\alpha_o Z_o}\Bigg(\frac{\sqrt{2}\alpha_o^2\alpha_s^2 J_2(\tilde{\alpha}_s)}{\tilde{\alpha}_s(\alpha_f^2 - \alpha_s^2)(\tilde{\alpha}_s J_0(\tilde{\alpha}_s) - J_1(\tilde{\alpha}_s))} - \frac{2\alpha_o^2 J_2(\tilde{\alpha}_s)}{\sqrt{\varepsilon_s}\tilde{\alpha}_s J_1(\tilde{\alpha}_s)} + \frac{\sqrt{2}(I_0(\alpha_s) - I_2(\alpha_s))(\alpha_f^2\delta_s - \alpha_s^2(\delta_s - 1))}{(\alpha_f^2 - \alpha_s^2)(I_0(\alpha_s) + I_2(\alpha_s))} \\ &+ \frac{4\sqrt{\varepsilon_s}\{\alpha_f^2(I_1(\alpha_s) - \alpha_s I_0(\alpha_s))[(\alpha_o^2 + \alpha_s^2)J_1(\tilde{\alpha}_s) - \alpha_o^2\tilde{\alpha}_s J_0(\tilde{\alpha}_s)] + \alpha_s^2(\alpha_o^2 - \alpha_s^2)I_1(\alpha_s)(J_1(\tilde{\alpha}_s) - \tilde{\alpha}_s J_0(\tilde{\alpha}_s))\}}{\alpha_s\tilde{\alpha}_s(\alpha_s^2 - \alpha_f^2)(\alpha_s^2 - \alpha_o^2)(I_0(\alpha_s) + I_2(\alpha_s))(J_0(\tilde{\alpha}_s) - J_2(\tilde{\alpha}_s))}\Bigg)\mathcal{W}_{\mathrm{TMs}}(\tilde{\alpha}_{fs}) \\ &+ -\frac{2\alpha_f}{Z_f\sqrt{\varepsilon_s}\tilde{\alpha}_{fs}}\mathcal{W}_{\mathrm{TMs}}{}'(\tilde{\alpha}_{fs})\Bigg].\end{aligned} \tag{C15}$$

$$\mathrm{T4}_{ss} = b\alpha_s\sqrt{\frac{2}{\pi}}\sqrt{\frac{\epsilon_s}{L}}, \tag{C16}$$

$$\mathrm{T5}_{s\,s} = \frac{2b\alpha_o^2\alpha_s}{\sqrt{\pi}\sqrt{L}}, \tag{C17}$$

$$\mathrm{G4}_{s\,p} = \frac{1}{\sqrt{\beta_p^2 - 1}\beta_{p\,s}^2}, \tag{C18}$$

$$\mathrm{G5}_{s\,p} = \frac{1}{\sqrt{\beta_p^2 - 1}\beta_{p\,s}^2(\alpha_o^2 - \beta_{p\,s}^2)}, \tag{C19}$$

$$\mathrm{F3}_{s\,s} = \frac{\alpha_f(\delta_s - 1)\tilde{\alpha}_s^2[J_0(\tilde{\alpha}_s) + J_2(\tilde{\alpha}_s)]}{Y_f\alpha_o Z_o\tilde{\alpha}_{fs}[J_0(\tilde{\alpha}_s) - J_2(\tilde{\alpha}_s)]}\mathcal{W}'_{\mathrm{TEs}}(\tilde{\alpha}_{fs}) + \mathcal{W}_{\mathrm{TEs}}(\tilde{\alpha}_{fs}), \tag{C20}$$

$$\mathrm{F4}_{s\,s} = \frac{j\alpha_s(\alpha_o^2 - \alpha_f^2)[J_0(\tilde{\alpha}_s) + J_2(\tilde{\alpha}_s)]}{\alpha_o Z_o\tilde{\alpha}_{fs}^2[J_0(\tilde{\alpha}_s) - J_2(\tilde{\alpha}_s)]}\mathcal{W}_{\mathrm{TMs}}(\tilde{\alpha}_{fs}). \tag{C21}$$

APPENDIX D: MATRIX ELEMENTS—IMPEDANCE

$$Z_{1\,p}^{I,C_{\mathrm{TM}}} = \frac{jb(\tilde{\alpha}_p + \beta\alpha_o)}{\sqrt{2\pi}\alpha_p^2 J_0(\alpha_p)(\tilde{\alpha}_p + \alpha_b)}, \tag{D1}$$

$$Z_{1\,p}^{I,C_{\mathrm{TE}}} = \frac{-jb(\beta\tilde{\beta}_p + \alpha_o)}{\sqrt{2\pi}Y_o\beta_p^2\sqrt{\beta_p^2 - 1}J_0(\beta_p)(\tilde{\beta}_p + \alpha_b)}, \tag{D2}$$

$$Z_{1\,p}^{II,D_{\mathrm{TM}}} = \frac{-jbe^{\frac{jL\alpha_b}{b}}(\beta\alpha_o - \tilde{\alpha}_p)}{\sqrt{2\pi}\alpha_p^2 J_0(\alpha_p)(\alpha_b - \tilde{\alpha}_p)}, \tag{D3}$$

$$Z_{1\,p}^{II,D_{\mathrm{TE}}} = \frac{jbe^{\frac{jL\alpha_b}{b}}(\alpha_o - \beta\tilde{\beta}_p)}{\sqrt{2\pi}Y_o\beta_p^2\sqrt{\beta_p^2 - 1}J_0(\beta_p)(\alpha_b - \tilde{\beta}_p)}. \tag{D4}$$

$$Z_{1\,p}^{IV_{\mathrm{TM}},C_{\mathrm{TM}}} = \frac{b[\alpha_b\alpha_p^2[-\cot(\frac{L\tilde{\alpha}_p}{b}) + e^{\frac{jL\alpha_b}{b}}\csc(\frac{L\tilde{\alpha}_p}{b})] + j\tilde{\alpha}_p(\alpha_b^2 - \alpha_o^2)]}{\sqrt{2\pi}\alpha_b\alpha_p^2 J_2(\alpha_p)(\alpha_b^2 - \alpha_o^2 + \alpha_p^2)}, \tag{D5}$$

$$Z_{1\,p}^{IV_{\mathrm{TM}},D_{\mathrm{TM}}} = \frac{b\{j\tilde{\alpha}_p e^{\frac{jL\alpha_b}{b}}(\alpha_b^2 - \alpha_o^2) + \alpha_b\alpha_p^2[-\csc(\frac{L\tilde{\alpha}_p}{b}) + e^{\frac{jL\alpha_b}{b}}\cot(\frac{L\tilde{\alpha}_p}{b})]\}}{\sqrt{2\pi}\alpha_b\alpha_p^2 J_2(\alpha_p)(\alpha_b^2 - \alpha_o^2 + \alpha_p^2)}, \tag{D6}$$

$$Z_{1\,s}^{IV_{\mathrm{TM}},A_{\mathrm{TM}}} = \frac{jb(-1 + (-1)^s e^{\frac{jL\alpha_b}{b}})}{(\alpha_b^2 - \alpha_s^2)\sqrt{\frac{L}{\epsilon_s}}}\left(\frac{\tilde{\alpha}_s}{2J_1(\tilde{\alpha}_s)} - 1\right)\mathcal{W}_{\mathrm{TMs}}(\tilde{\alpha}_{fs}). \tag{D7}$$

$$Z_{1\,p}^{IV_{\mathrm{TE}},C_{\mathrm{TE}}} = \frac{b\sqrt{L}\alpha_o\{j\alpha_b + \beta_p\mathrm{csch}(\frac{L\beta_p}{b})[\cosh(\frac{L\beta_p}{b}) - e^{\frac{jL\alpha_b}{b}}]\}}{\sqrt{2\pi}Y_o\beta_p^2\sqrt{L(\beta_p^2 - 1)}J_0(\beta_p)(\alpha_b^2 + \beta_p^2)}, \tag{D8}$$

$$Z_{1\,p}^{IV_{\mathrm{TE}},D_{\mathrm{TE}}} = -\frac{b\alpha_o\{L\beta_p\mathrm{csch}(\frac{L\beta_p}{b}) + jLe^{\frac{jL\alpha_b}{b}}[\alpha_b + j\beta_p\coth(\frac{L\beta_p}{b})]\}}{\sqrt{2\pi}\sqrt{L}Y_o\beta_p^2\sqrt{L(\beta_p^2 - 1)}J_0(\beta_p)(\alpha_b^2 + \beta_p^2)}, \tag{D9}$$

$$Z_{1\,s}^{IV_{\mathrm{TE}},A_{\mathrm{TE}}} = \frac{\sqrt{2}b\alpha_f\alpha_s(\delta_{\mathrm{s0}} - 1)(-1 + (-1)^s e^{\frac{jL\alpha_b}{b}})\mathcal{W}'_{\mathrm{TEs}}(\tilde{\alpha}_{fs})}{\sqrt{L}Y_f(\alpha_s^2 - \alpha_b^2)[I_0(\alpha_s) + I_2(\alpha_s)]\tilde{\alpha}_{fs}}, \tag{D10}$$

$$Z_{1\,s}^{IV_{\mathrm{TE}},A_{\mathrm{TM}}} = \frac{jb\sqrt{\epsilon_s}(-1 + (-1)^s e^{\frac{jL\alpha_b}{b}})(\alpha_f^2(\frac{1}{I_0(\alpha_s) + I_2(\alpha_s)} - 1) + \alpha_s^2)\mathcal{W}_{\mathrm{TMs}}(\tilde{\alpha}_{fs})}{\sqrt{L}(\alpha_b^2 - \alpha_s^2)\tilde{\alpha}_{fs}^2}. \tag{D11}$$

$$Z_{1\,p}^{IV_H,C_{\mathrm{TE}}} = \frac{b\alpha_o Z_o(\alpha_b\mathrm{csch}(\frac{L\beta_p}{b})(-\cosh(\frac{L\beta_p}{b}) + e^{\frac{jL\alpha_b}{b}}) + j\beta_p)}{\sqrt{2\pi}\alpha_b\beta_p\sqrt{\beta_p^2 - 1}J_0(\beta_p)(\alpha_b^2 + \beta_p^2)}, \tag{D12}$$

$$Z_{1\,p}^{IV_H,D_{\mathrm{TE}}} = \frac{b\beta Z_o[\alpha_b\mathrm{csch}(\frac{L\beta_p}{b}) - e^{\frac{jL\alpha_b}{b}}(\alpha_b\coth(\frac{L\beta_p}{b}) + j\beta_p)]}{\sqrt{2\pi}\beta_p\sqrt{\beta_p^2 - 1}J_0(\beta_p)(\alpha_b^2 + \beta_p^2)}, \tag{D13}$$

$$Z_{1\,s}^{IV_H,A_{\mathrm{TE}}} = -\frac{b\beta^2\alpha_f\alpha_s\beta_s^2\epsilon_s(-1 + (-1)^s e^{\frac{jL\alpha_o}{b\beta}})\mathcal{W}'_{\mathrm{TEs}}(\tilde{\alpha}_{fs})}{\sqrt{2}\sqrt{L}Y_f[2\beta_s I_1(\beta_s) - 2\beta_s^2 I_0(\beta_s)]\tilde{\alpha}_{fs}(\beta^2\alpha_s^2 - \alpha_o^2)}, \tag{D14}$$

$$Z_{1\,s}^{IV_H,A_{\mathrm{TM}}} = -\frac{jb\beta\alpha_b\beta_s^2\epsilon_s(-1 + (-1)^s e^{\frac{jL\alpha_b}{b}})((\delta_{\mathrm{s0}} + 1)\tilde{\alpha}_{fs}^2 + \alpha_s^2)\mathcal{W}_{\mathrm{TMs}}(\tilde{\alpha}_{fs})}{2\alpha_o(\alpha_b^2 - \alpha_s^2)\sqrt{\frac{L}{\epsilon_s}}[2\beta_s I_1(\beta_s) - 2\beta_s^2 I_0(\beta_s)]\tilde{\alpha}_{fs}^2}. \tag{D15}$$

[1] H. Henke, Point charge passing a resonator with beam tubes, Arch. Elektrotech. **69**, 271 (1986).

[2] K. Bane and B. Zotter, Transverse modes in periodic cylindrical cavities, in *11th International Conference on High-Energy Accelerators*, edited by W. S. Newman, Experientia Supplementum Vol. 40, 581–585 (Birkhäuser, Basel, 1980).

[3] S. Krinsky, B. Podobedov, and R. L. Gluckstern, Impedance of finite length resistive cylinder, Phys. Rev. ST Accel. Beams **7**, 114401 (2004).

[4] G. Stupakov, Resistive wall impedance of an insert, Phys. Rev. ST Accel. Beams **8**, 044401 (2005).

[5] Y. Shobuda, Y. H. Chin, and K. Takata, Coupling impedances of a resistive insert in a vacuum chamber, Phys. Rev. ST Accel. Beams **12**, 094401 (2009).

[6] Y. Shobuda, Y. H. Chin, and K. Takata, Impedance of a ceramic break and its resonance structures, Phys. Rev. ST Accel. Beams **17**, 091001 (2014).

[7] T. Weiland, BCI—a computer program for transient electromagnetic fields of bunched beams in accelerators, CERN, Geneva, Technical Report No. CERN-ISR-TH-80-45, 1980.

[8] T. Weiland, TBCI and URMEL—New computer codes for wake field and cavity mode calculations, IEEE Trans. Nucl. Sci. **30**, 2489 (1983).

[9] T. Weiland, Transverse beam cavity interaction. Part I: Short range forces, Nucl. Instrum. Methods Phys. Res. **212**, 13 (1983).

[10] Y. H. Chin, Y. Shobuda, and K. Takata, ABCI Progresses and Plans: Parallel Computing and Transverse Napoly-Shobuda Integral, in *Proceedings of the 22nd Particle Accelerator Conference, PAC-2007, Albuquerque, NM* (IEEE, New York, 2007), pp. 3306–3308.

[11] I. Zagorodnov, Computation of electromagnetic fields generated by relativistic beams in complicated structures, in *Proceedings of North American Particle Accelerator Conference, NAPAC'16, Chicago, IL* (2016), WEA1IO02, pp. 642–646, https://jacow.org/napac2016/papers/wea1io02.pdf.

[12] N. Biancacci, V. Vaccaro, E. Métral, B. Salvant, M. Migliorati, and L. Palumbo, Impedance studies of 2D azimuthally symmetric devices of finite length, Phys. Rev. ST Accel. Beams **17**, 021001 (2014).

[13] G. Franceschetti, *Electromagnetics: Theory, Techniques, and, Engineering Paradigms* (Springer Science & Business Media, New York, 1997).

[14] J. G. Van Bladel, *Electromagnetic Fields, 2nd ed.* (Wiley, Newark, 2007).

[15] R. L. Gluckstern, Analytic methods for calculating coupling impedances, Report No. CERN-2000-011, CERN, Geneva, Switzerland, CERN Yellow Reports: Monographs, 2000.

[16] MATLAB, *9.7.0.1190202 (R2019b)* (The MathWorks Inc., Natick, MA, 2018).

[17] R. Mittra, Relative convergence of the solution of a doubly infinite set of equations, J. Res. Natl. Bur. Stand., Sect. D **67D**245 (1963).

[18] A. W. Chao, K. H. Mess, M. Tigner, and F. Zimmermann, *Handbook of Accelerator Physics and Engineering*, 2nd ed. (World Scientific, Singapore, 2013).

[19] K. Y. Ng, Transverse impedance of a coasting beam in a corrugated vacuum chamber at low frequencies, FERMILAB, Batavia, IL, Technical Report No. FERMILAB-FN-0389, 1983.

[20] A. W. Chao, *Physics of Collective Beam Instabilities in High Energy Accelerators* (John Wiley & Sons, Inc., New York, 1993).

[21] N. Mounet and E. Métral, Electromagnetic fields created by a macroparticle in an infinitely long and axisymmetric multilayer beam pipe, CERN, Geneva, Switzerland, Technical Report No. CERN-BE-2009-039, 2009.

[22] Dassault Système: CST—Computer Simulation Technology GmbH: CST Studio Suite. Version 2022, http://www.cst.com/.

[23] G. V. Stupakov and S. S. Kurennoy, Trapped electromagnetic modes in a waveguide with a small discontinuity, Phys. Rev. E **49**, 794 (1994).

[24] E. T. Jaynes, Ghost modes in imperfect waveguides, Proc. IRE **46**, 416 (1958).

[25] L. Palumbo, V. G. Vaccaro, and M. Zobov, Wake fields and impedance, LNF, Rome, Italy, Report No. LNF-94/041, 1994, arXiv:physics/0309023.

[26] F. Zimmermann and K. Oide, Resistive-wall wake and impedance for nonultrarelativistic beams, Phys. Rev. ST Accel. Beams **7**, 044201 (2004).

[27] N. Biancacci, LEIR KEM impedance study, in *49th Impedance Working Group Meeting, CERN, Geneva, Switzerland* (2021), https://indico.cern.ch/event/1040326/.